

Contents lists available at ScienceDirect

Petroleum Science

journal homepage: www.keaipublishing.com/en/journals/petroleum-science



Original Paper

Numerical simulation of gas kick evolution and wellbore pressure response characteristics during the deepwater dual gradient drilling



Geng Zhang ^a, Hong-Wei Yang ^{a, *}, Jun Li ^{a, b}, Hui Zhang ^a, Hong-Lin Huang ^c, Biao Wang ^a, Wen-Xu Wang ^a. Hao Chen ^d

- ^a China University of Petroleum-Beijing, Changping, 102249, Beijing, China
- ^b China University of Petroleum-Beijing at Karamay, Karamay, 834000, Xinjiang, China
- ^c CNOOC Hainan Branch, Engineering & Technical Operation Center, Haikou, 570100, Hainan, China
- ^d CNPC Xinjiang Oilfield Company, Research Institute of Engineering Technology, Karamay, 834000, Xinjiang, China

ARTICLE INFO

Article history: Received 29 April 2024 Received in revised form 9 December 2024 Accepted 9 December 2024 Available online 12 December 2024

Edited by Jia-Jia Fei

Keywords:
Gas kick
Multiphase flow
Dual gradient drilling
Equivalent circulating density
Downhole separator

ABSTRACT

The gas kick represents a major risk in deepwater oil and gas exploration. Understanding the dynamics of gas kick evolution and the associated pressure response characteristics is critical for effective well control. In this paper, we introduce a transient wellbore multiphase flow model specifically developed to simulate gas kick in deepwater dual-gradient drilling, incorporating a downhole separator. The model accounts for the variable mass flow within the annulus and heat exchange between the annular fluid and the formation. Using this model, we analyzed the multiphase flow and thermodynamic behavior during the gas kick. Simulation results reveal a progressive increase in bottom-hole temperature, underscoring its potential as a key indicator for gas kick early detection. Additionally, variable gradient parameters affect not only the annular equivalent circulating density (ECD) profile but also the evolution of the gas kick. The inclusion of a downhole separator alters the annular ECD profile, creating a "broken line" shape, which enhances adaptability to the multi-pressure systems typically encountered in deepwater formation. By adjusting factors such as hollow sphere concentration, separator position, and separation efficiency, the annular ECD profile can be effectively customized. This study provides important theoretical insights and practical applications for utilizing dual-gradient drilling technology to address challenges in deepwater formation drilling.

© 2024 The Authors. Publishing services by Elsevier B.V. on behalf of KeAi Communications Co. Ltd. This is an open access article under the CC BY license (http://creativecommons.org/licenses/by/4.0/).

1. Introduction

The deepwater oil and gas formation is set to become the primary focus of future exploration due to the global depletion of high-quality resources in shallower formation. These deepwater formation is characterized by complex pressure systems and distinct thermal environments, posing significant challenges to conventional drilling (CD). Among these challenges are a narrow safe pressure window, low predictive accuracy of wellbore pressure, and an increased risk of gas kick (Zhang et al., 2015; Nayeem et al., 2016; Jiang et al., 2019).

The managed pressure drilling (MPD) technology has emerged as an effective solution for addressing drilling challenges in formation with multiple pressure systems. MPD represents a

* Corresponding author. E-mail address: zerotone@cup.edu.cn (H.-W. Yang). comprehensive system engineering approach that integrates measurement, interpretation, and control (Nas et al., 2010; Kaasa et al., 2012). To date, MPD has evolved into two primary methods: constant bottom-hole pressure and dual gradient drilling (DGD). While the former method has been successfully applied in shallow water formations, its effectiveness in deepwater formations remains limited (Santos et al., 2003). Recently, to address the challenge of narrow safe pressure windows in deepwater settings, Gao et al. (2016) introduced the novel concept of variable gradient managed pressure drilling, as shown in Fig. 1. This innovative method utilizes segmented control of annular fluid density, combining constant bottom-hole pressure with DGD, and demonstrates significant adaptability to deepwater environments.

As a novel drilling technique, this method differs significantly from traditional drilling practices, and its underlying theoretical framework remains underdeveloped. The behavior of wellbore multiphase flow and heat transfer during gas kick in DGD is still poorly understood. The multiphase flow presents a dynamic and

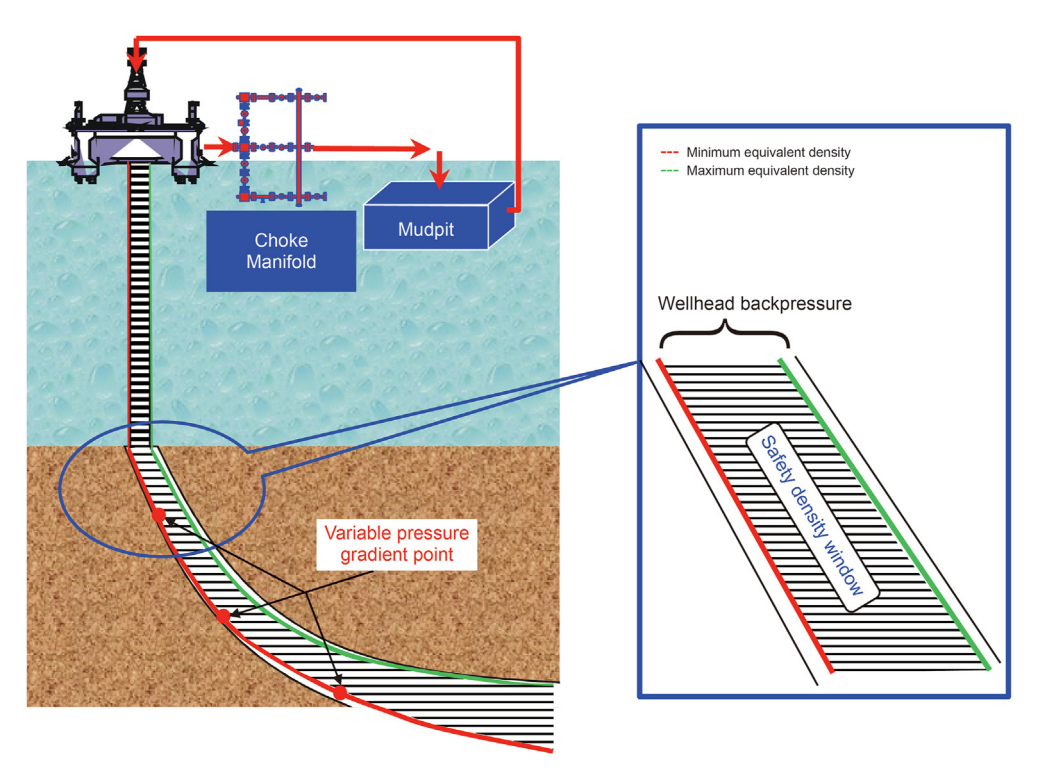


Fig. 1. Schematic diagram of variable gradient managed pressure drilling.

complex challenge, involving variable mass flow influenced by numerous factors, such as gas slip, heat exchange, variations in fluid physical properties, and the interaction between temperature and pressure.

The current multiphase flow models include the homogeneous fluid model (HFM), the two-fluid model (TFM), and the drift flux model (DFM) (Choi et al., 2013). Compared to the HFM and TFM, the DFM accounts for gas slip and variations in gas volume fraction and velocity across the flow cross-section, significantly reducing computational errors while simplifying the solution process. The DFM was first introduced by Zuber and Findlay (1965) and has since been widely adopted. Ekrann and Rommetveit (1985) were the first to apply the DFM to simulate the behavior of wellbore multiphase flow during gas kick. Many scholars have since expanded the DFM's application to simulate gas kick evolution. To date, extensive research on multiphase flow behavior has been conducted from both theoretical and experimental perspectives (Avelar et al., 2009; Dixit and ElSheikh, 2022; Hibiki et al., 2022).

The experimental research on multiphase flow has been extensive, with notable studies dating back to 1997 when Lopes conducted full-scale multiphase flow experiments at the University of Louisiana, simulating the evolution of gas kick (Lopes, 1997). In 2003, the University of Tulsa performed experiments using large-scale inclined wells to investigate the impact of variables such as drill string rotation, wellbore inclination, and wellhead pressure on multiphase flow behavior (Sunthankar et al., 2001). Additionally, Lorentzen et al. (2001) conducted full-scale experiments to examine changes in bottom-hole pressure during gas kick. Most recently, Yang et al. (2017) carried out laboratory experiments on multiphase flow at high gas kick rates and analyzed pressure response characteristics at various well depths.

The numerical simulation of gas kick has undergone significant development. Nunes et al. (2002) developed a mathematical model for simulating gas kick during deepwater drilling, considering factors such as wellbore structure, pressure loss, and gas expansion.

Schubert et al. (2006) created a multiphase flow model for multibranch horizontal wells and analyzed wellbore pressure response characteristics. Kinik et al. (2015) utilized the DFM to study gas kick evolution. He et al. (2017) examined the dissolution of acidic gas in water-based drilling fluid using the TFM. Xu et al. (2018) developed a non-isothermal transient multiphase model that incorporated the influence of the geothermal gradient. Yang et al. (2020) established a non-isothermal multiphase model focused on annular variable mass flow. Zachopoulos and Kokkinos (2023) developed a comprehensive gas kick simulation method that accounted for flow friction, heat transfer effects, and gas dissolution. Zhang et al. (2024) used Fluent software to simulate gas kick in deep fractured reservoirs and analyzed the effects of fracture width, fracture number, and drilling fluid properties on gas kick evolution.

Additionally, numerous scholars have developed multiphase flow models that focus on gas kick detection (Choe et al., 2007; Nas, 2011; Karimi Vajargah et al., 2013; Li et al., 2022; Yin et al., 2022), initial gas kick response (Davoudi et al., 2011; Smith and Patel, 2012; Wang et al., 2016; Yang et al., 2022a), and well control (Dou et al., 2012; Chen et al., 2018; Gomes et al., 2018). The existing literature indicates that research on wellbore multiphase flow models is extensive, and the accuracy of these models has continually improved, largely meeting the engineering requirements of the CD. However, despite these advancements, the models exhibit significant deficiencies in two main areas: (1) The common application of wellbore multiphase flow models to the CD fails to account for variations in mass flow and channel diameters, leading to substantial computational errors in the DGD. (2) Although current models account for non-isothermal conditions, they neglect the impact of the Joule-Thomson effect on thermal convection.

To address these shortcomings, this paper develops a mathematical model specifically designed for the DGD utilizing a downhole separator. The model enables the investigation of gas kick evolution and wellbore pressure response characteristics. The paper is structured into three main sections: (1) The first section

outlines the fundamental principles of DGD and details the model development process. (2) The second section explains the model solution process and validation. (3) The final section simulates gas kick evolution and analyzes the impact of variable gradient parameters on wellbore multiphase flow behaviors. Finally, the paper presents its findings and draws comprehensive conclusions from the research.

2. Basic principles of DGD based on downhole separator

The key to achieving multiple pressure gradients within the wellbore lies in the strategic injection of lightweight hollow spheres at one or more points along the annulus. According to the literature, four primary tools facilitate the injection of hollow spheres: double-wall drill pipe, an additional pipeline, lined casing, and a cyclone separator. Among these, the cyclone separator stands out for its ability to dynamically adjust pressure gradients. It requires fewer auxiliary devices, is simpler to implement, and offers a wider range of pressure adjustments within the annulus. As a result, this paper focuses on utilizing the cyclone separator to achieve the DGD, as illustrated in Fig. 2.

The DGD system, which incorporates a cyclone separator, connects to one or more cyclone separators integrated into the drill string. At the wellhead, both the drilling fluid and hollow spheres are pumped into the drill string. As the mixed fluid travels down the drill string to the separator, centrifugal force separates the hollow spheres into the annulus, thereby creating multiple pressure gradients within it. Fig. 3 illustrates the DGD process using a downhole separator.

3. Mathematical model

Fig. 4 illustrates the multiphase flow process in DGD. The variable gradient parameters, including hollow sphere concentration, separation efficiency, separator position, and the number of separators, significantly influence the behavior of multiphase flows within the annulus. These variations, in turn, can impact the

evolution of gas kick.

To accurately simulate gas kick evolution in DGD, it is essential to fully consider the variable mass flow in the annulus. Additionally, this paper addresses the heat transfer between the drilling fluid and the formation. Subsequently, a non-isothermal, fully transient multiphase flow model was established. The model is based on the following assumptions.

- (1) The wellbore flow is treated as one-dimensional, and the radial behavior of the drilling fluid is disregarded.
- (2) In vertical wellbore, the temperature is consistent across all phases at the same cross-section.
- (3) Apart from the separator location, the hollow spheres and drilling fluid within the annulus are assumed to be uniformly mixed.

3.1. Multiphase flow model

When the mixed fluid passes through a stationary control volume unit, the mass conservation equations for each phase within the control volume unit are expressed as follows:

$$\begin{split} \frac{\partial}{\partial t} \left(A \rho_{\rm g} \alpha_{\rm g} \right) + \frac{\partial}{\partial z} \left(A \rho_{\rm g} \alpha_{\rm g} \nu_{\rm g} \right) &= q_{\rm g} \\ \frac{\partial}{\partial t} \left(A \rho_{\rm l} \alpha_{\rm l} + A \rho_{\rm s} \alpha_{\rm s} \right) + \frac{\partial}{\partial z} \left(A \rho_{\rm l} \alpha_{\rm l} \nu_{\rm l} + A \rho_{\rm s} \alpha_{\rm s} \nu_{\rm s} \right) &= q_{\rm s} \end{split} \tag{1}$$

where, ρ is density, kg/m³; α is volume fraction, dimensionless; A is cross-sectional area of the annulus, m²; ν is velocity, m/s; q_g is gas kick rate, kg/(s·m); q_s is hollow ball transfer rate, kg/(s·m); t is time, s; t is axial displacement, m. The subscripts g, l and s represent gas, drilling fluid and hollow sphere respectively.

During the gas kick, the multiphase flow process within the wellbore is highly unstable. Continuous changes in the distribution of each phase can significantly impact the wellbore pressure profile. The momentum conservation equation for the mixed fluid is expressed as follows:





Fig. 2. The cyclone separator sub and guide vanes.

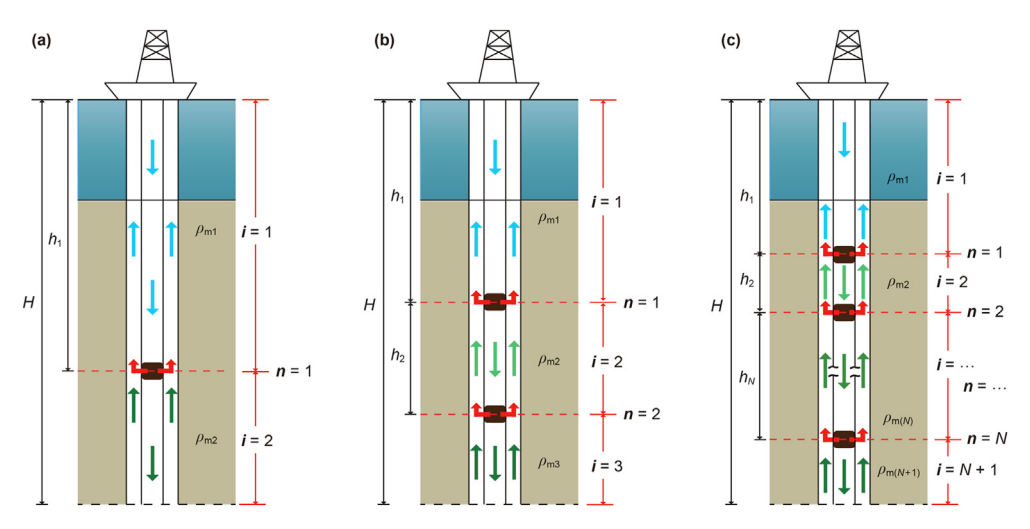


Fig. 3. The process of DGD based on downhole separator.

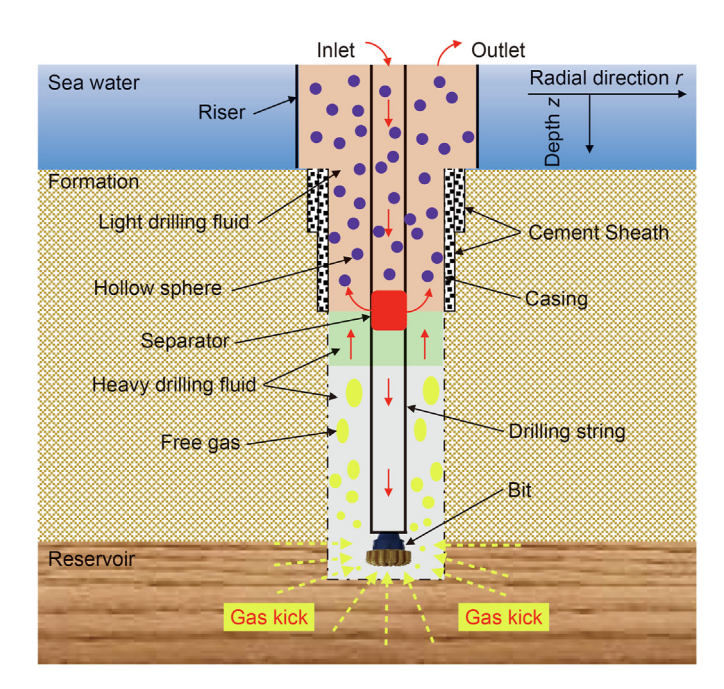


Fig. 4. The process of multiphase flow of DGD.

$$\begin{split} &\frac{\partial}{\partial t} \left(\sum_{i} A \rho_{i} \alpha_{i} \nu_{i} \right) + \frac{\partial}{\partial z} \left(\sum_{i} A \rho_{i} \alpha_{i} \nu_{i}^{2} \right) + \frac{\partial}{\partial z} (Ap) \\ &= - \sum_{i} A f \frac{\rho_{i} \alpha_{i} \nu_{i}^{2}}{2 d_{hy}} - \sum_{i} A \rho_{i} \alpha_{i} g \sin \theta - q_{g} \nu_{g} - q_{s} \nu_{l} \quad i = g, l, s \end{split}$$

$$(2)$$

where, p is pressure, Pa; f is friction coefficient, dimensionless; $d_{\rm hy}$ is hydraulic diameter, m; g is acceleration of gravity, m/s²; θ is hole drift angle, rad.

3.2. Thermodynamic model

The thermophysical properties of each phase are influenced by the wellbore temperature. Conversely, the multiphase flow process also affects the wellbore temperature. As a result, the evolution of gas kick is a dynamic process, which induces continuous changes in wellbore temperature.

According to the first law of thermodynamics, and taking into account the gas Joule-Thomson effect, heat exchanges between the drilling fluid and the formation, as well as heat convection involving both the invading gas and the drilling fluid, and between the hollow spheres and the drilling fluid, the transient heat transfer equation in the annular is as follow:

$$\begin{split} &\frac{\partial}{\partial t} \left[\sum_{i} A \rho_{i} \alpha_{i} \left(U_{i} + v_{i}^{2} / 2 \right) \right] + \frac{\partial}{\partial z} \left[\sum_{i} A \rho_{i} \alpha_{i} v_{i} \left(U_{i} + v_{i}^{2} / 2 \right) \right] \\ &= Q_{\text{ex}} + Q_{\text{conv}}^{g} + Q_{\text{conv}}^{s} + \sum_{i} A f \frac{\rho_{i} \alpha_{i} v_{i}^{2}}{2 d_{\text{hy}}} v_{i} - \sum_{i} A \rho_{i} \alpha_{i} v_{i} g \sin \theta \ i = \text{g,l,s} \end{split}$$

$$(3)$$

where, U is internal energy, J/kg; $Q_{\rm ex}$ is heat exchange term, J/(m·s); $Q_{\rm conv}^{\rm g}$ is thermal convection term of gas and drilling fluid, J/(m·s); $Q_{\rm conv}^{\rm g}$ is thermal convection term between hollow sphere and drilling fluid, J/(m·s).

During the drilling process, the drilling fluid heat exchanges with the surrounding formation, casing wall, riser, and drill string wall, which can be expressed as:

$$Q_{\rm ex} = A\lambda_{\rm m} \left(\frac{\partial^2 T}{\partial r^2} + \frac{1}{r} \frac{\partial T}{\partial r} \right) \tag{4}$$

Here, $\lambda_{\rm m}$ is mixed fluid thermal conductivity, W/(m·°C); T is temperature, °C; r is radial displacement, m.

Interphase heat convection occurs between the invading gas and drilling fluid, and can be expressed as:

$$Q_{\text{conv}}^{g} = q_{g} \left[C_{pg} \left(T_{f,ave} - T \right) - C_{pg} C_{J} \left(p_{f,ave} - p \right) \right]$$
 (5)

Here, C_{pg} is specific heat of gas, J/(kg·°C); C_{J} is Joule Thomson coefficient, °C/Pa; $p_{f,ave}$ is average formation pressure, Pa; $T_{f,ave}$ is average formation temperature, °C.

When the separator releases the hollow spheres from inside the drill string into the annulus, heat convection occurs between the hollow spheres and the annulus fluid, and can be expressed as:

$$Q_{\text{conv}}^{s} = q_{s}C_{ps}(T_{p} - T) \tag{6}$$

Here, C_{ps} is specific heat of hollow sphere, J/(kg·°C); T_p is temperature inside drill string, °C.

There is single-phase flow in the drill string, the heat transfer equation in drill string as follows:

$$\frac{\partial}{\partial t} \left[\sum_{i} A \rho_{i} \alpha_{i} \left(U_{i} + v_{i}^{2} / 2 \right) \right] + \frac{\partial}{\partial z} \left[\sum_{i} A \rho_{i} \alpha_{i} v_{i} \left(U_{i} + v_{i}^{2} / 2 \right) \right]
= Q_{\text{ex}} + \sum_{i} A f \frac{\rho_{i} \alpha_{i} v_{i}^{2}}{2 d_{\text{hy}}} v_{i} - \sum_{i} A \rho_{i} \alpha_{i} v_{i} g \sin \theta \quad i = l, s$$
(7)

The formation temperature primarily depends on three factors: (1) the rate of heat conduction in both the radial and axial directions; (2) the rate of heat exchange between the formation pore fluid and the rock matrix; (3) the thermal expansion effect on the formation pore fluid (Farahani et al., 2006). Consequently, the heat transfer model within the formation can be expressed as follows:

$$c_0 = \frac{A_e}{1 + (A_e - 1)\gamma^2} \tag{10}$$

Here, $A_{\rm e}$ is empirical coefficient, dimensionless; γ is attenuation coefficient, dimensionless.

The gas slip velocity v_{∞} is:

$$\nu_{\infty} = \frac{c_0 \nu_{\rm c} (1 - \alpha_{\rm g} c_0) K(\alpha_{\rm g})}{1 - \alpha_{\rm g} c_0 \left[1 - (\rho_{\rm g}/\rho_{\rm l})^{1/2} \right]} (\cos \theta)^{1/2} (1 + \sin \theta)^2$$
 (11)

where, $K(\alpha_g)$ is gas phase characteristic parameter, dimensionless; v_c is gas phase characteristic velocity, m/s.

The mass transfer rate of hollow spheres is a critical parameter, primarily influenced by liquid phase displacement, separation efficiency, and the hollow spheres density. Yang et al. (2022b) derived the calculating equation for the mass transfer rate based on the separation efficiency tests of the cyclone separator, as illustrated below:

$$\left[\phi(\rho C)_{pl} + (1 - \phi)(\rho C)_{f}\right] \left(\frac{dT}{dt}\right)_{f} = \lambda_{ef} \left(\frac{\partial^{2}T}{\partial r^{2}} + \frac{1}{r}\frac{\partial T}{\partial r} + \frac{\partial^{2}T}{\partial z^{2}}\right)_{f} - \phi(\rho C \nu)_{pl} \left(\frac{\partial T}{\partial r}\right)_{f} - (\beta_{T}K_{T})_{pl} \left[\left(\frac{\nu}{r} + \frac{\partial \nu}{\partial r}\right)_{pl}(T)_{f} + (\nu)_{pl} \left(\frac{\partial T}{\partial r}\right)_{f}\right]$$
(8)

$$q_{s(n)} = \frac{\partial}{\partial z} \left(\eta_{s(n)} \rho_s q_1 \right) = \frac{\rho_{m(i+1)} - \rho_{m(i)}}{\rho_L - \rho_{m(1)}} \frac{\partial}{\partial z} (\rho_s q_1) \quad (n = 1, 2, ..., N \quad i = n)$$
(12)

where, ϕ is formation porosity, dimensionless; C is specific heat, $J/(kg\cdot {}^{\circ}C)$; $\lambda_{\rm ef}$ is formation effective thermal conductivity, $W/(m\cdot {}^{\circ}C)$; $\beta_{\rm T}$ is thermal expansion coefficient of formation fluid, $1/{}^{\circ}C$; $K_{\rm T}$ is isothermal bulk elastic modulus, Pa. The subscripts pl and f represent pore fluid and formation, respectively.

3.3. Auxiliary equations

The DFM effectively characterizes the non-uniform profile of gas velocity and phase distribution, a fact that has been thoroughly validated by numerous prior studies (Livescu et al., 2010; Tang et al., 2018; Sun et al., 2019). In terms of the flow section, the gas velocity can be described as follows:

$$v_{g} = c_{0} \left(\alpha_{g} v_{g} + \alpha_{l} v_{l} \right) + v_{\infty} \tag{9}$$

where, c_0 is gas distribution coefficient, dimensionless; v_{∞} is gas slip velocity, m/s.

The numerous studies (Johnson and Cooper, 1993; Bhagwat and Ghajar, 2014) have focused on c_0 and v_∞ . Shi et al. (2005) derived an empirical equation for the distribution coefficient and slip rate using extensive indoor experimental data, which has gained widespread recognition in the oil and gas industry.

The gas distribution coefficient c_0 is:

Here, η_s is separation efficiency of separator, dimensionless; q_l is drilling fluid flow rate, m^3/s ; ρ_m is mixed fluid density, kg/m^3 . The subscript i indicates the i-th separator position.

The gas migration within the wellbore leads to a continual decrease in bottom-hole pressure, which subsequently causes a gradual increase in the gas invasion rate. To estimate this rate, a transient reservoir model is employed, as outlined below (Sun et al., 2017):

$$q_{\rm g}(t) = \frac{2\pi K h \left[p_{\rm e}^2 - p_{\rm b}^2 \right]}{\mu_{\rm g} \ln \frac{2.25K t / \mu_{\rm g} C_{\rm t}}{r_{\rm w}^2}} \frac{T_{\rm b} Z_{\rm b}}{p_{\rm b} Z_{\rm e} T_{\rm e}} \rho_{\rm g}$$
(13)

where, K is permeability, D; h is reservoir opening thickness, m; p_e is reservoir pressure, Pa; p_b is bottom hole pressure, Pa; T_e is reservoir temperature, °C; T_b is bottom hole temperature, °C; Z_e is gas compression factor under reservoir, dimensionless; Z_b is gas compression factor under bottom hole, dimensionless; μ_g is gas viscosity, Pa·s; C_t is overall compressibility, 1/Pa; r_w is borehole radius, m.

The gas kick is a dynamic process characterized by constantly changing phase composition. As a result, the rate of heat exchange between the annular fluid and the surrounding environment is also subject to dynamic changes, a factor often overlooked in earlier multiphase flow models. Gao et al. (2018) developed a model based on the Nusselt number.

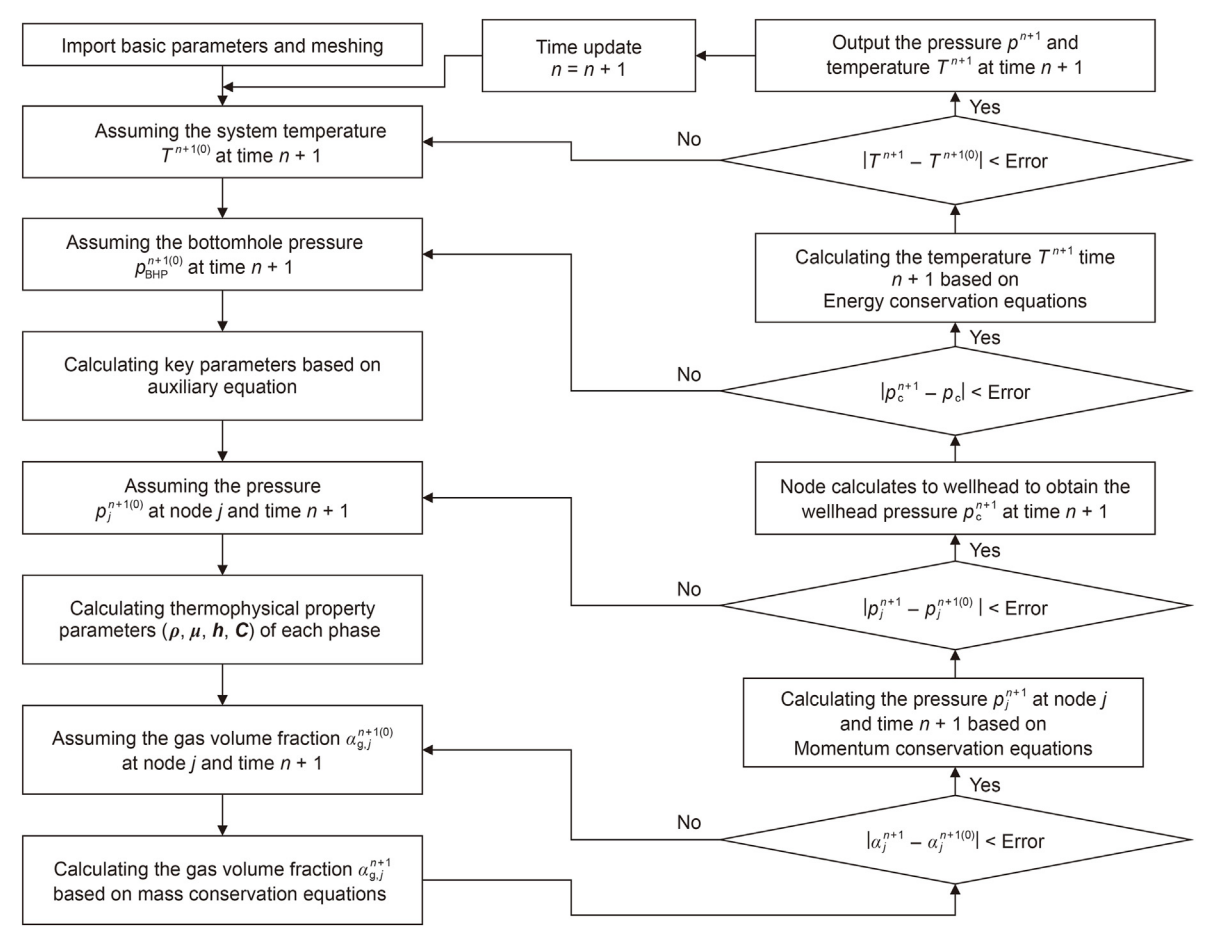


Fig. 5. The model solving flow diagram.

Table 1 Basic experimental parameters.

Parameters	Value
Depth, m	1793
Inner diameter of casing, m	0.2184
Outer diameter of pipe, m	0.0889
Inner diameter of pipe, m	0.066
Fluid density, kg/m ³	1140
Fluid viscosity, Pa·s	0.012
Flow rate, L/s	13.2
Gas invasion rate, m ³ /s	0.45

$$\textit{Nu} = 0.01215 \textit{Re}^{0.7922} \, \textit{Pr}^{0.3} \textit{C}_{T} \Big(1 - 0.30577 \alpha_{g}^{-0.16578} \Big) \eqno(14)$$

Here, Nu is Nussel number, dimensionless; Re is Reynolds number, dimensionless; Pr is Prandtl number, dimensionless; C_T is temperature correction factor, dimensionless.

Chen (1979) proposed that the friction coefficient is mainly determined by the Reynolds number of mixed fluids, namely:

$$f = \begin{cases} \frac{16}{Re}, Re \le 2100\\ \left[4\log\left(\frac{\Delta/d_{\text{hy}}}{3.7065}\right)\right] - \frac{5.0452}{Re}\log A, Re > 2100 \end{cases}$$
 (15)

where, Δ is wall roughness, dimensionless; Λ is intermediate

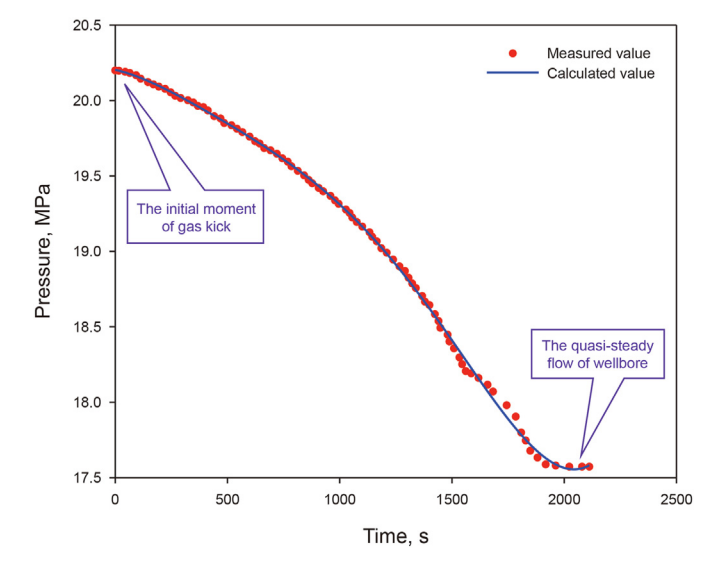


Fig. 6. The measured pressure changes over time at position 1768 m.

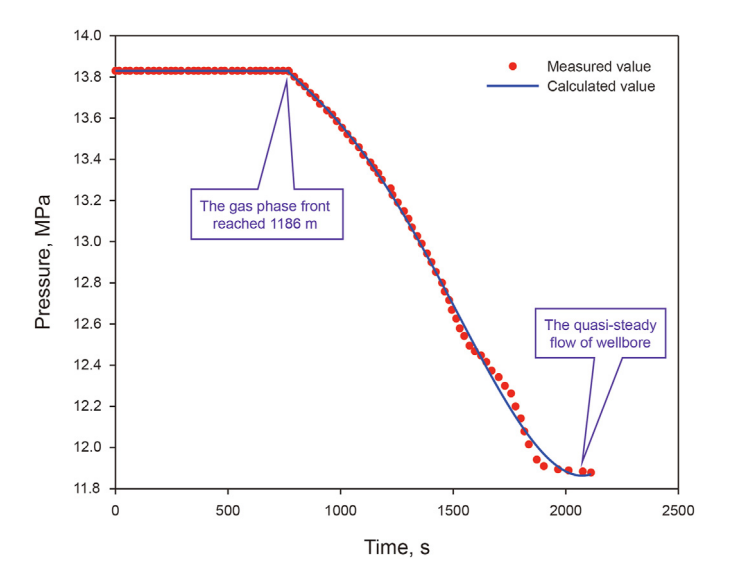
parameter, dimensionless.

4. Model solving and validation

4.1. Initial and boundary conditions

At the initial moment, before the onset of gas kick, the wellbore





Gas fraction, % 10 15 20 1000 2000 Depth, m 3000 t = 1500 s 4000 t = 3000 s t = 4500 s t = 5300 s5000 t = 5800 s t = 6000 sDual gradient drilling 6000 Conventional drilling

Fig. 7. The measured pressure changes over time at position 1186 m.

Fig. 9. The gas phase volume fraction profile of DGD and CD under different times.

Table 2The basic parameters for simulation.

Parameter	Value	Parameter	Value
Well depth, m	6000	Thermal conductivity of drilling fluid, W/(m·K)	1.73
Sea depth, m	1500	Specific heat of drilling fluid, J/(kg·°C)	1650
Drilling fluid density, kg/m ³	1550	Thermal conductivity of seawater, W/(m·K)	0.85
Drilling fluid viscosity, Pa·s	0.060	Specific heat of seawater, J/(kg·°C)	4100
Pump rate, m ³ /s	0.025	Thermal conductivity of rock, W/(m·K)	2.23
Surface temperature, °C	15	Specific heat of rock, J/(kg·°C)	850
Inlet temperature, °C	20	Thermal conductivity of drill string, W/(m·K)	55.2
Geothermal gradient, °C/m	0.024	Specific heat of drill string, J/(kg·°C)	450
Formation permeability, µm ²	0.032	Thermal conductivity of cement, W/(m·K)	0.76
Seawater density, kg/m ³	1025	Specific heat of cement, J/(kg·°C)	1000
Rock density, kg/m ³	2600	Thermal conductivity of gas, W/(m·K)	0.035
Rate of penetration, m/h	20	Specific heat of gas, J/(kg·°C)	1015
Inner diameter of drill pipe, mm	127.0	Drill pipe outer diameter, mm	152.0
Inner diameter of drill collar, mm	66.1	Drill collar outer diameter, mm	152.0
Inner diameter of riser, mm	508.0	Bit diameter, mm	215.9
Hollow sphere concentration	40%	Separator position, m	3000
Separation efficiency	100%	Formation supply radius, m	200
Hollow sphere density, kg/m ³	345	Wellhead backpressure, MPa	0.5

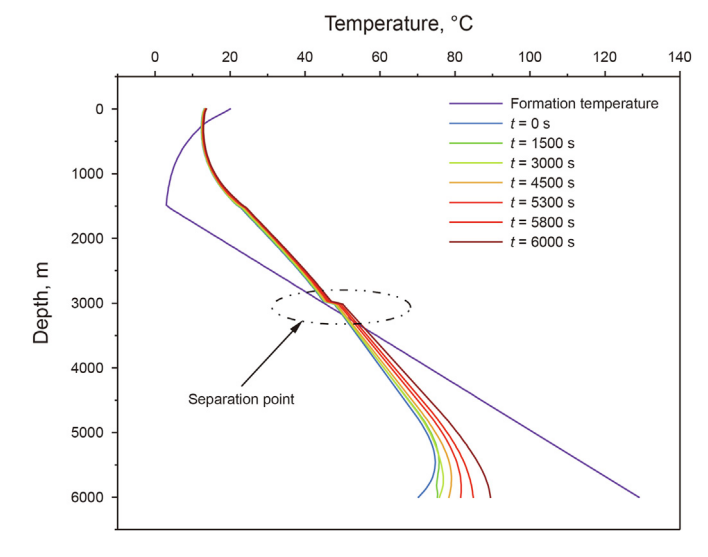


Fig. 8. The annular temperature profile under different times.

experiences single-phase flow. Consequently, the initial temperature and pressure profile of the wellbore is established based on the stable circulation conditions typically observed during normal operations.

$$T(i,j,0) = T_{\text{norm}}(i,j,0)$$
 (16)

$$p(j,0) = p_{\text{norm}}(j) \tag{17}$$

Here, $T_{\rm norm}$ is wellbore temperature of CD, °C; $p_{\rm norm}$ is wellbore pressure of CD, Pa.

For DGD, the wellhead backpressure is known as the pressure boundary condition.

$$p(0,t) = p_{c} \tag{18}$$

Here, p_c is wellhead backpressure, Pa.

The temperature of the injected drilling fluid can be directly measured as the temperature boundary condition.

$$T_{\mathbf{p}}(0,t) = T_{\mathbf{in}} \tag{19}$$

Here, $T_{\rm in}$ is injected drilling fluid temperature, $^{\circ}$ C.

Al Saedi et al. (2018) used the field-measured data to evaluate various boundary conditions and found that when the gradient of bottom-hole temperature along the axis was set to zero, the calculated bottom-hole temperature showed the best agreement with the measured data. The DGD shares the same bottom-hole boundary condition as CD.

$$\frac{\mathrm{d}T(H,t)}{\mathrm{d}z} = 0\tag{20}$$

Here, H is bottom hole depth, m.

4.2. Model solving method and process

The fully transient, non-isothermal multiphase flow model exhibits strong nonlinearity. The model's governing equations are discretized using a fully implicit finite difference scheme (Yin et al., 2017; Sun et al., 2018). In this study, an iterative method was employed to solve the system of linear equations, with the detailed

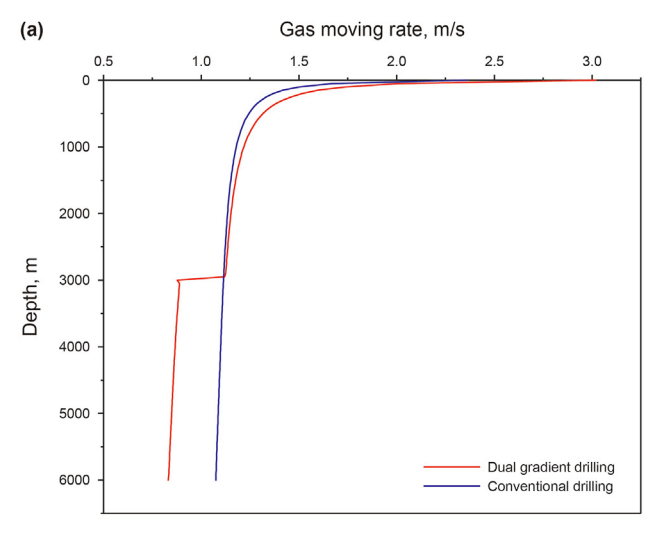
calculation process illustrated in Fig. 5.

4.3. Model validation

Direct validation of the model with measured data is currently challenging because the DGD technology, which relies on a downhole separator, remains theoretical. However, the model can also predict the wellbore pressure for the CD when variable mass flow is disregarded. Therefore, it is feasible to indirectly verify the model's accuracy using experimental data from CD scenarios involving gas kick.

This paper validates the accuracy and reliability of the model using pressure data measured in a full-scale experimental well at the University of Louisiana (Lopes, 1997). In the experimental setup, pressure gauges were positioned at depths of 1768 and 1186 m, allowing for real-time measurement of annular pressure. The experimental well is vertical, with key parameters detailed in Table 1. Pressure readings of 17.61 and 11.81 MPa were recorded at 1768 and 1186 m, respectively, under quasi-steady flow conditions.

Figs. 6 and 7 display the simulation results of pressure changes over time at depths of 1768 and 1186 m, respectively. According to these figures, after gas migrates from the bottom hole to the



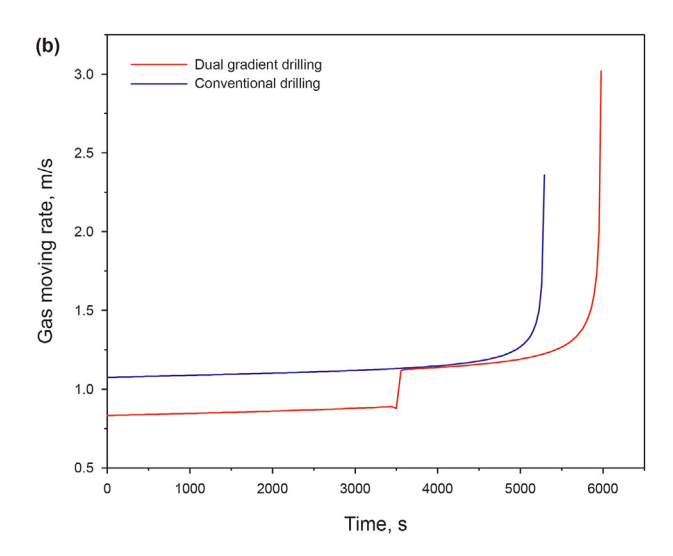
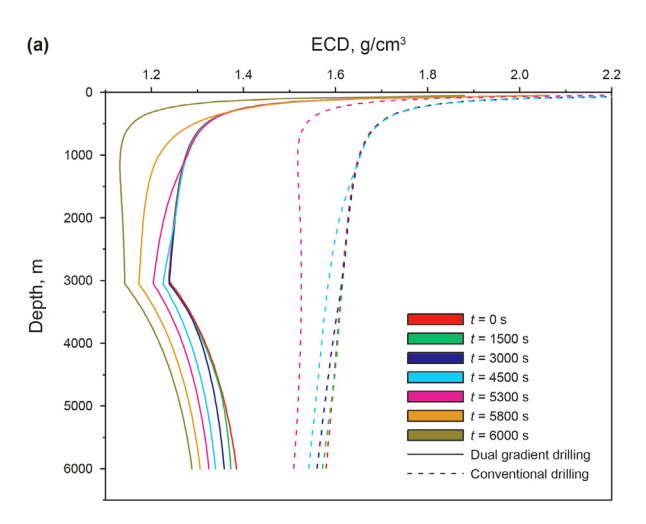


Fig. 10. The gas migration velocity profile of DGD and CD.



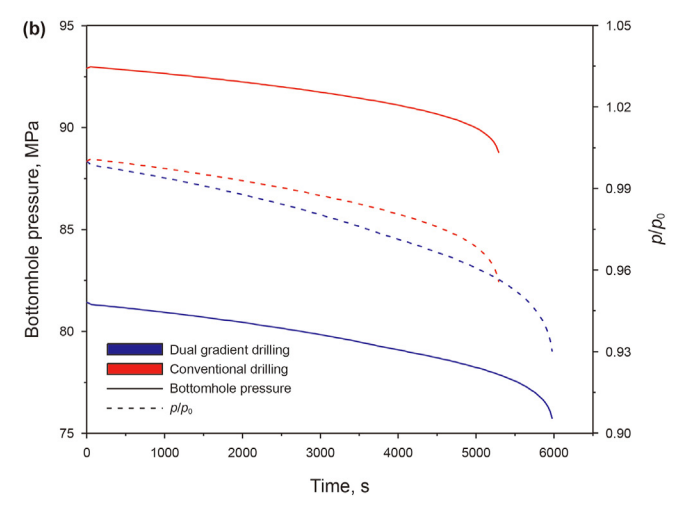


Fig. 11. The ECD profile and bottom hole pressure over time curve of DGD and CD.

wellhead, the wellbore pressure stabilizes, and the flow state transitions from transient to quasi-steady. The calculated pressures at 1768 and 1186 m under quasi-steady flow conditions are 17.56 and 11.87 MPa, respectively, closely matching the measured data. These results demonstrate the model's accuracy and reliability when compared with actual measurements.

5. Results and discussions

To simulate the evolution of gas kick and the corresponding wellbore pressure response characteristics in the DGD, this study performed a series of calculations using the developed model. By comparing these results with the CD, this study analyzed the impact of variable gradient parameters on gas kick evolution. The basic parameters are detailed in Table 2.

5.1. Wellbore temperature profile

Fig. 8 illustrates the annular temperature profile at various times during gas kick. As time progresses, the annular temperature gradually increases due to axial heat convection caused by the upward flow of high-temperature fluid from the bottom of the well. However, as the well depth decreases, the rate of temperature increase diminishes. This effect occurs because the wellbore fluid progressively transfers heat to the formation and the drill string, reducing heat convection within the annular fluid. Additionally, at

the separation point, low-temperature hollow spheres are separated and enter the annulus, inducing thermal convection with the high-temperature drilling fluid. This interaction causes a sudden temperature drop along the flow direction in the annulus, creating a distinct change point.

5.2. Wellbore multiphase flow behaviors

5.2.1. Gas volume fraction

Fig. 9 displays the gas phase volume fraction profiles for DGD and CD at various times. The figure shows that after gas kick, gas enters the annulus and continuously migrates upward. Before reaching the wellhead, the gas phase volume fraction in the annulus initially increases and then gradually declines until it nearly reaches zero. Additionally, due to the continuous separation of hollow spheres into the annulus at the separator position, the annulus flow rate increases, and the volume fraction of drilling fluid decreases. Consequently, as the gas migrates upward to the separator position, the gas volume fraction in the wellbore suddenly drops.

Below the separator, the flow rate in DGD is lower than in CD, resulting in a higher gas migration velocity in CD during gas kick. Consequently, when the circulation times are identical, the gas front in CD will advance ahead of that in DGD. Additionally, above the separator, the annular mixed fluid density in DGD is lower than in CD, leading to a higher bottom hole gas invasion rate in DGD

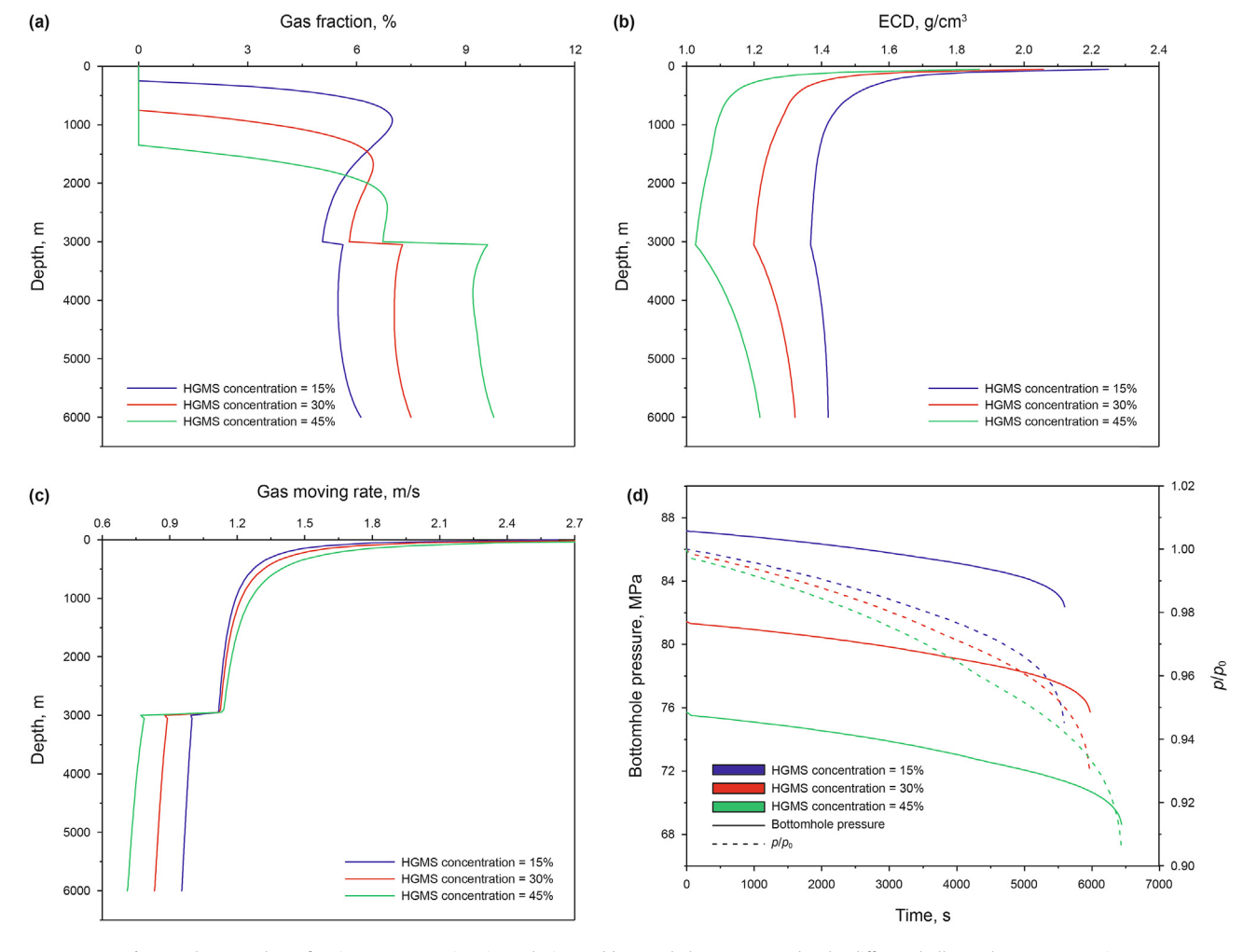


Fig. 12. The gas volume fraction, ECD, gas migration velocity, and bottom hole pressure under the different hollow sphere concentration.

compared to CD. Therefore, near the bottom hole, the gas phase volume fraction is greater in DGD than in CD.

5.2.2. Gas migration rate

Fig. 10(a) and (b) display the gas migration velocity profiles of DGD and CD during gas kick. The figures show that the gas migration velocity gradually increases from the bottom hole to the wellhead as the well depth decreases. Additionally, as time progresses, this velocity continues to increase. Above the separator, the gas migration velocity in DGD exceeds that in CD due to the release of hollow spheres into the annulus through the separator, which accelerates the fluid velocity and results in a sharp increase in gas migration velocity along the flow direction. However, at the same well depth, before the gas reaches the separator position, the velocity in DGD consistently remains lower than in CD. This suggests that after the gas kick, it takes longer for the gas to reach the separator position in DGD than in CD, providing additional time for gas kick detection and well control operations, which enhances drilling safety. This is one of the advantages of the DGD.

5.2.3. Wellbore pressure profile

Fig. 11 displays the ECD profile and the bottom hole pressure curve over time for DGD and CD. Due to the influence of wellhead backpressure, the ECD near the wellhead changes rapidly. However, this section of the ECD, typically within the riser, does not impact

drilling safety. Near the mud line, the ECD gradient reverses under both drilling methods, primarily because the fluid moves from the formation annulus into the riser annulus, leading to a sudden increase in wellbore size and a significant reduction in friction loss. Unlike CD, the ECD profile for DGD shows a turning point at the separator position, below which the ECD gradually increases with well depth. Ignoring the dramatic changes in ECD near the wellhead, the overall ECD profile in DGD approximates a 'broken line' shape, which better accommodates the narrow safety density window of deep-water formations compared to CD.

As time progresses, the gas gradually migrates upwards and expands, resulting in a gradual decrease in bottom hole pressure. Consequently, the ECD also decreases as the duration of gas invasion increases. Additionally, the continual introduction of low-density hollow spheres into the annulus means that the rate of bottom hole pressure reduction in DGD to be more pronounced than in CD.

5.3. Discussions

Extensive research has been conducted on conventional sensitivity parameters such as reservoir pressure, reservoir permeability, temperature, wellbore structure, and pump rate in previous studies. The conclusions drawn from these studies are also applicable to DGD. Therefore, this paper examines the effects of variable gradient parameters (hollow spheres concentration, separation

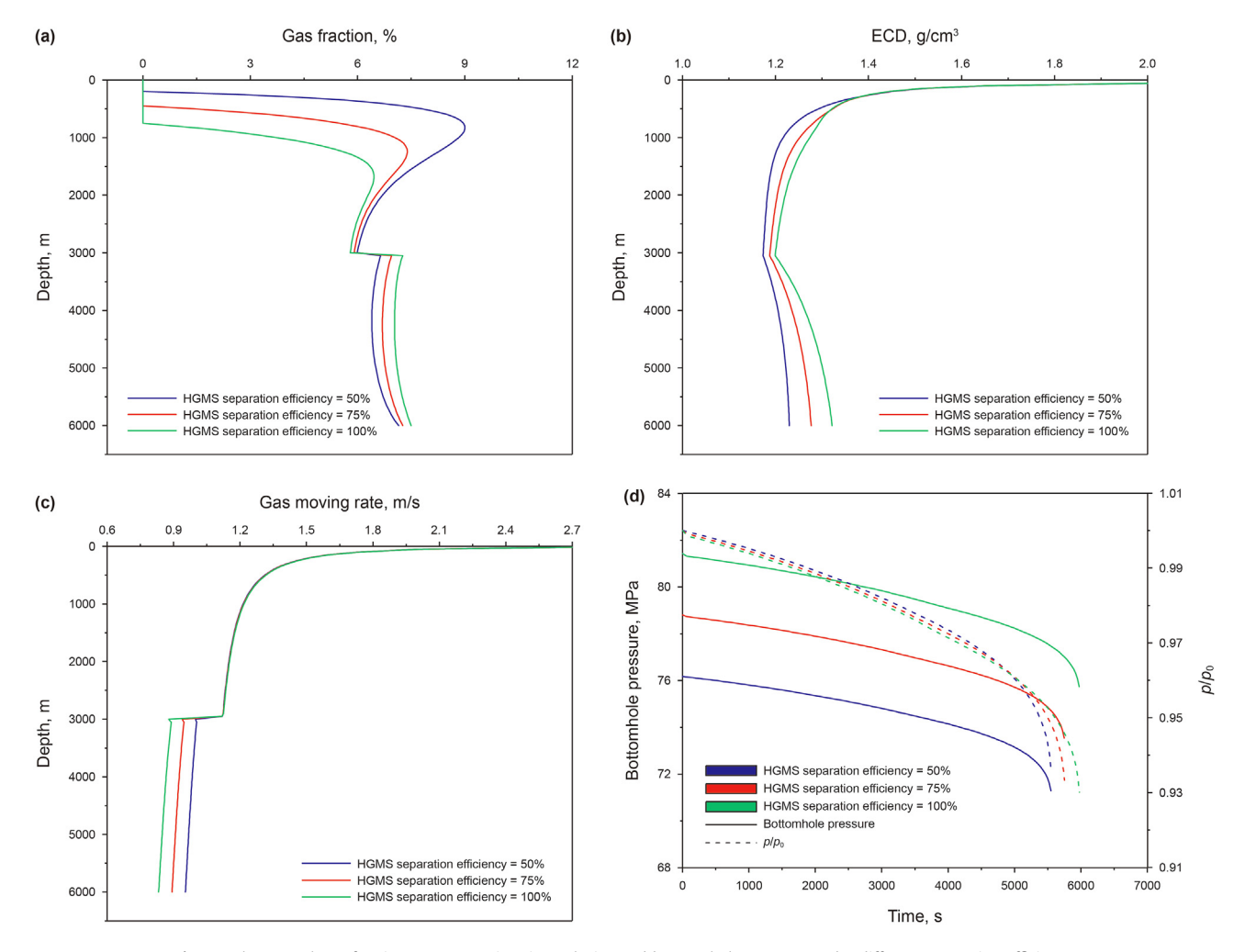


Fig. 13. The gas volume fraction, ECD, gas migration velocity, and bottom hole pressure under different separation efficiency.

efficiency, separation point position, and the number of separators) on wellbore multiphase flow behaviors under identical initial and boundary conditions.

5.3.1. Hollow sphere concentration

Fig. 12(a)—(d) illustrate the gas phase volume fraction profile, ECD profile, gas migration velocity profile, and bottom hole pressure variation curve at hollow sphere concentrations of 15%, 30%, and 45%, respectively. When the initial bottom hole pressure difference is the same, a higher hollow sphere concentration results in a lower mixed fluid density above the separator, and consequently, a reduced bottom hole pressure. This leads to an accelerated gas invasion rate and a larger gas volume fraction below the separator, as depicted in Fig. 12(a). Additionally, a higher concentration of hollow spheres correlates with a reduced flow rate below the separator, increased gas migration velocity, and an extended well section traversed by the gas within the same time frame, as illustrated in Fig. 12(c).

Moreover, due to the high concentration of hollow spheres, both the gas volume fraction and the gas invasion rate are relatively high. This results in a corresponding decrease in ECD at the same depth, leading to a more pronounced 'broken line' profile, as illustrated in Fig. 12(b). Consequently, the rate of decrease in bottom hole pressure accelerates over time, as depicted in Fig. 12(d). Therefore, these observations suggest that adjusting the

concentration of hollow spheres can effectively regulate the ECD profile.

5.3.2. Separation efficiency

Fig. 13(a)—(d) display the gas phase volume fraction profile, ECD profile, gas migration velocity profile, and bottom hole pressure variation curve at separation efficiencies of 50%, 70%, and 100%, respectively. Separation efficiency primarily influences the annulus fluid density and flow rate below the separator. When the initial bottom hole pressure difference is consistent, lower separation efficiencies correspond to reduced fluid densities below the separator and increased gas migration velocities. Consequently, this leads to more extensive gas movement within the same duration and a higher gas phase volume fraction above the separator, as illustrated in Fig. 13(a) and (c).

Furthermore, an increase in the gas volume fraction leads to a rapid rise in the rate of bottom hole pressure difference, which in turn accelerates the gas invasion rate. Consequently, below the separator, as the separation efficiency decreases, the rate of bottom hole pressure reduction increases correspondingly, and the ECD at the same well depth gradually decreases, making the 'broken line' profile less distinct, as shown in Fig. 13(b) and (d). This demonstrates that the separation efficiency primarily influences the ECD profile below the separator position.

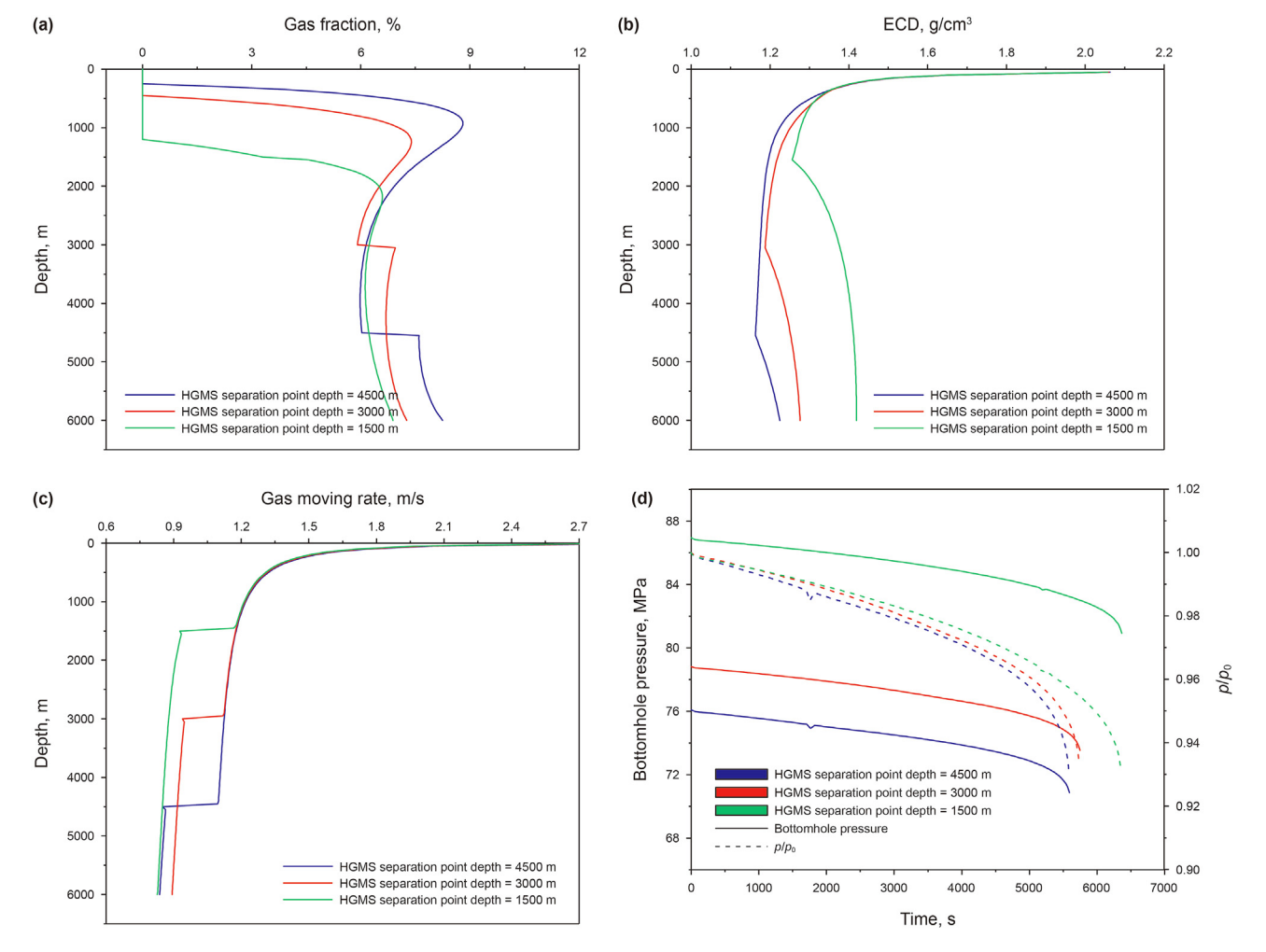


Fig. 14. The gas volume fraction, ECD, gas migration velocity, and bottom hole pressure under different separation point position.

5.3.3. Separation point position

Fig. 14(a)—(d) illustrate the gas phase volume fraction profile, ECD profile, gas migration velocity profile, and bottom hole pressure variation curve at separator depths of 1500, 3000, and 4500 m, respectively. As the depth at which the separator is positioned decreases, it results in a longer annular well section with slower flow velocity below the separator, which in turn reduces the gas migration velocity, as depicted in Fig. 14(c). Conversely, this reduction in depth shortens the fluid section with lower density above the separator, leading to a slower rate of bottom hole pressure decrease and a smaller gas volume fraction, as illustrated in Fig. 14(a) and (d).

Furthermore, when the basic simulation parameters are identical, the greater the distance between the separator and the drill bit, the higher the ECD is at the corresponding well depth below it, as illustrated in Fig. 14(b). This suggests that the position of the separator not only adjusts the ECD but also determines the specific adjustment point based on the characteristics of the safety pressure window. As previously analyzed, the ECD profile can be flexibly adjusted by varying the position of the separator, its separation efficiency, and the concentration of hollow balls.

5.3.4. Number of separators

As illustrated in Fig. 15(a)—(d), the analysis shows that the impact of the number of separators on wellbore multiphase flow behaviors integrates multiple effects, including separator position, separation efficiency, and hollow ball concentration. However, the influence of separator position is predominant. Consequently, the effect of the number of separators on multiphase flow behaviors aligns closely with the impact of separator position. The variations in gas volume fraction, gas migration velocity, and bottom hole pressure reduction rate across different numbers of separators are minimal.

Additionally, as the number of separators increases from the bottom upwards, the ECD at the same well depth below the lowermost separator position also gradually increases. Theoretically, adjusting both the number and position of separators can allow the ECD to conform to various complex and narrowly defined safety pressure windows. However, a greater number of separators necessitates control over more key parameters, thereby increasing the complexity of managing wellbore pressure. Therefore, under current conditions, it is advisable to opt for a single separator.

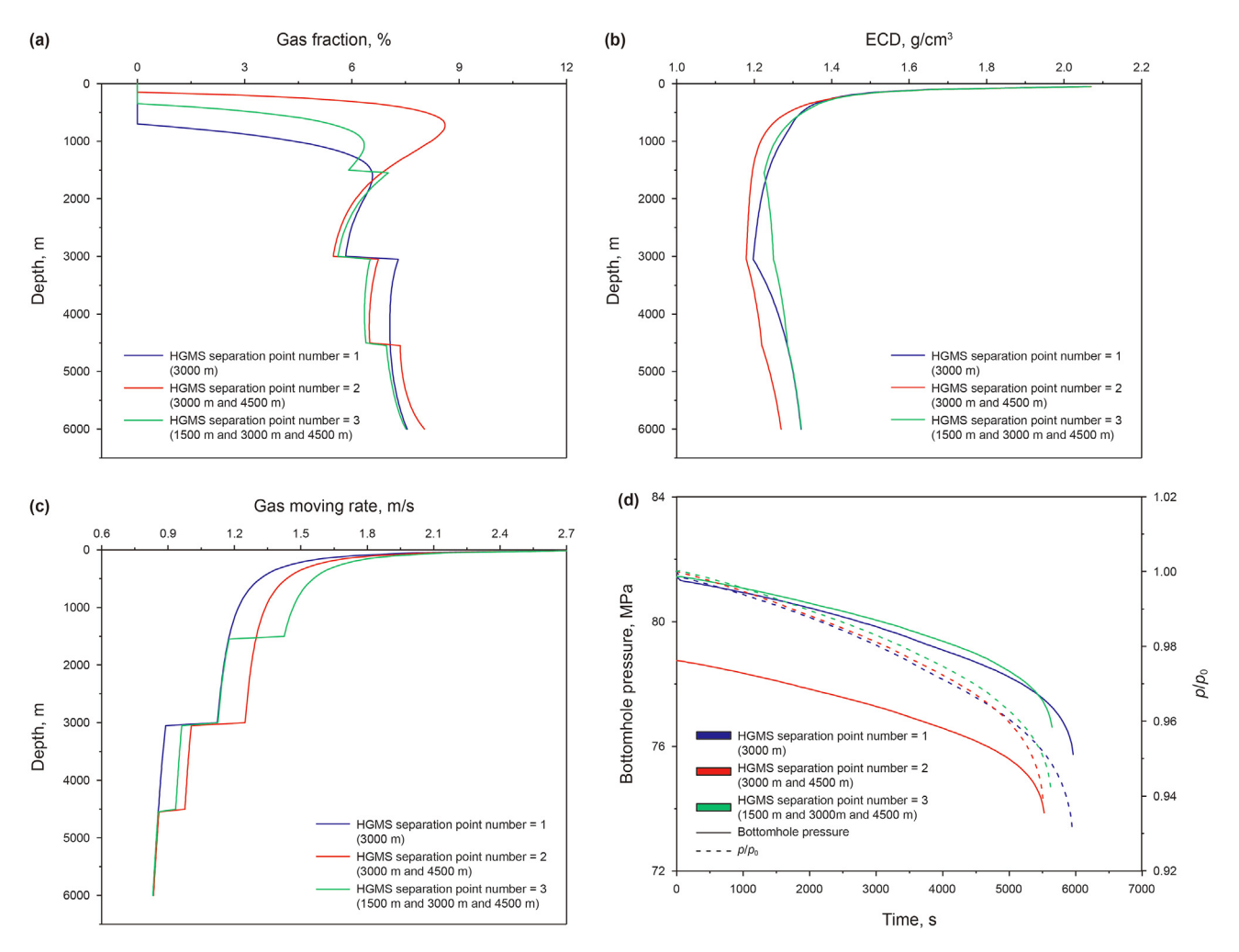


Fig. 15. The gas volume fraction, ECD, gas migration velocity, and bottom hole pressure under different number of separators.

6. Conclusions

A new non-isothermal transient multiphase flow model for DGD was developed, incorporating the effects of variable mass flow in the annulus due to gradient parameters and heat transfer between the drilling fluid and the surrounding environment. This model was used to analyze the evolution of gas kick and the corresponding wellbore pressure response characteristics. The main research conclusions are summarized as follows.

- (1) The gas invading the annulus undergoes thermal convection, causing the annulus temperature to gradually increase. However, once the gas kick rate exceeds a certain threshold, the Joule-Thomson effect becomes the dominant factor influencing the bottom hole temperature, resulting in a gradual decrease in the rate of temperature increase. Additionally, changes in bottom hole temperature can serve as a diagnostic feature for detecting gas kick.
- (2) When the initial bottom hole pressure difference remains constant, variable gradient parameters influence multiphase flow behaviors by affecting annular friction loss. Similarly, when the formation pressure remains unchanged, these parameters impact multiphase flow behaviors by altering the bottom hole pressure difference.
- (3) In DGD, hollow spheres effectively reduce the fluid density above the separator, causing the ECD in the annulus to approximate a 'broken line' profile. The interplay of hollow spheres concentration, separation efficiency, and separator location allows for flexible adjustment of the annulus ECD profile, providing substantial adaptability within the complex and narrow safety pressure window.

CRediT authorship contribution statement

Geng Zhang: Writing — review & editing, Writing — original draft, Software, Resources, Funding acquisition. Hong-Wei Yang: Writing — original draft, Resources, Funding acquisition. Jun Li: Resources, Funding acquisition. Hui Zhang: Writing — review & editing, Validation, Supervision. Hong-Lin Huang: Writing — review & editing. Biao Wang: Writing — review & editing. Wen-Xu Wang: Writing — review & editing. Hao Chen: Writing — review & editing.

Declaration of competing interest

The authors declare that they have no known competing financial interests or personal relationships that could have appeared to influence the work reported in this paper.

Acknowledgements

This research work was supported by the Postdoctoral Fellowship Program of CPSF (Grant No. GZC20233105), the Science Foundation of China University of Petroleum, Beijing (Grant No. 2462024XKBH006), the China Postdoctoral Science Foundation (Grant No. 2024M753615), the Major Scientific Research Instrument Development Program of National Natural Science

Foundation of China (Grant No. 52227804), and the Youth Science Foundation Program of National Natural Science Foundation of China (Grant No. 52404012).

Nomenclature

Nomenclature α volume fraction A cross-sectional area of the annulus, m² A _e empirical coefficient C _O gas distribution coefficient C _I Joule Thomson coefficient, K/Pa S _P specific heat, J/(Kg·K) C _I total compression coefficient, 1/Pa C _T temperature correction coefficient A _{hy} hydraulic equivalent diameter, m f firction coefficient φ formation porosity g gravitational acceleration, m²/s H enthalpy, J/Kg h thickness of the reservoir, m γ _S separation efficiency K(α _g) gas phase characteristic parameter K _T isothermal bulk leastic modulus, Pa A intermediate parameter Nu Nusselt number P wellbore pressure, Pa Pave.f average pressure of the invading gas, Pa Pb bottom hole pressure, Pa Pe reservoir pressure, Pa Pe reservoir pressure, Pa Pe reservoir pressure, Pa Pe reservoir pressure, Pa Pe wellbore pressure under normal condition, Pa Pr Prandtl number q mass flow rate, kg/(s·m) Q _{ex} heat exchange term, J Q ^g conv heat convection term between gas and drilling fluid, J Q ^g conv heat convection term between fluing fluid, K T _{norm} wellbore temperature of the invading gas, K T _e reservoir temperature under normal condition, K T _{norm} wellbore temperature of the invading gas, K T _e reservoir temperature under normal condition, K T _{norm} wellbore temperature of the invading gas, K T _e reservoir temperature under normal condition, K T _{norm} wellbore temperature of the invading gas, K reservoir temperature on the invading gas, K reservoir temperature on the invading thind, K Thorm wellbore temperature on the invading thind, K Thorm wellbore temperature on the invading thind, K Thorm wellbore temperature on the invadi		
A cross-sectional area of the annulus, m² Ae empirical coefficient Co gas distribution coefficient Cp specific heat, J/(kg·K) Ct total compression coefficient, 1/Pa CT temperature correction coefficient dhy hydraulic equivalent diameter, m f friction coefficient φ formation porosity g gravitational acceleration, m²/s H enthalpy, J/kg h thickness of the reservoir, m γ _b separation efficiency K reservoir permeability, D K (αg) gas phase characteristic parameter γ _c reservoir permeability, D K (αg) gas phase characteristic parameter Nu Nusselt number p wellbore pressure, Pa pave.f average pressure of the invading gas, Pa p _b bottom hole pressure, Pa p _c wellhead backpressure, Pa p _e reservoir pressure under normal condition, Pa Prandt number q Q _c heat convection term between pas and drilling fluid, I	Nomenclature	
$ \begin{array}{lll} A_{e} & & & & & & & & \\ C_{0} & & & & & & & \\ gas & & & & & & \\ C_{J} & & & & & & \\ Joule Thomson coefficient, K/Pa \\ Specific heat, J/Kg. K) \\ C_{t} & & & & & \\ total compression coefficient, 1/Pa \\ C_{T} & & & & & \\ total compression coefficient \\ d_{hy} & & & & \\ hydraulic equivalent diameter, m \\ f & & & \\ friction coefficient \\ \phi & & & \\ formation porosity \\ g & & & & \\ gravitational acceleration, m^{2}/s \\ H & & \\ enthalpy, J/kg \\ h & & \\ thickness of the reservoir, m \\ \eta_{5} & & & \\ separation efficiency \\ K & & \\ reservoir permeability, D \\ K (\alpha_g) & & \\ gas phase characteristic parameter \\ K_{T} & & \\ isothermal bulk elastic modulus, Pa \\ A & & \\ intermediate parameter \\ Nu & & \\ Nusselt number \\ p & & \\ wellbore pressure, Pa \\ p_{ave,f} & & \\ average pressure of the invading gas, Pa \\ p_{b} & & \\ bottom hole pressure, Pa \\ p_{e} & & \\ reservoir pressure under normal condition, Pa \\ P_{T} & & \\ p_{andst} & & \\ $	α	volume fraction
$ \begin{array}{lll} A_{e} & & & & & & & & \\ C_{0} & & & & & & & \\ gas & & & & & & \\ C_{J} & & & & & & \\ Joule Thomson coefficient, K/Pa \\ Specific heat, J/Kg. K) \\ C_{t} & & & & & \\ total compression coefficient, 1/Pa \\ C_{T} & & & & & \\ total compression coefficient \\ d_{hy} & & & & \\ hydraulic equivalent diameter, m \\ f & & & \\ friction coefficient \\ \phi & & & \\ formation porosity \\ g & & & & \\ gravitational acceleration, m^{2}/s \\ H & & \\ enthalpy, J/kg \\ h & & \\ thickness of the reservoir, m \\ \eta_{5} & & & \\ separation efficiency \\ K & & \\ reservoir permeability, D \\ K (\alpha_g) & & \\ gas phase characteristic parameter \\ K_{T} & & \\ isothermal bulk elastic modulus, Pa \\ A & & \\ intermediate parameter \\ Nu & & \\ Nusselt number \\ p & & \\ wellbore pressure, Pa \\ p_{ave,f} & & \\ average pressure of the invading gas, Pa \\ p_{b} & & \\ bottom hole pressure, Pa \\ p_{e} & & \\ reservoir pressure under normal condition, Pa \\ P_{T} & & \\ p_{andst} & & \\ $	Α	cross-sectional area of the annulus, m ²
$ \begin{array}{c} c_0 \\ C_1 \\ C_1 \\ Joule Thomson coefficient, K/Pa \\ C_p \\ Specific heat, J/(kg, K) \\ C_1 \\ C_1 \\ total compression coefficient, 1/Pa \\ C_2 \\ total compression coefficient dhy hydraulic equivalent diameter, m friction coefficient formation porosity g gravitational acceleration, m²/s enthalpy, J/kg h thickness of the reservoir, m \eta_s separation efficiency K reservoir permeability, D K(\alpha_g) gas phase characteristic parameter K_T isothermal bulk elastic modulus, Pa intermediate parameter Nu Nusselt number P wellbore pressure, Pa average pressure of the invading gas, Pa bottom hole pressure, Pa Pa wellbare pressure under normal condition, Pa Pr Prandtl number P Pa wellbare exchange term, Pa heat convection term between gas and drilling fluid, Pa Pa we.f Pa well so meat convection term between hollow ball and drilling fluid Pa Pa average temperature of the invading gas, Pa Pa Pa Pa Pa Pa Pa Pa$	A_e	
$ \begin{array}{c} C_j \\ C_p \\ Specific heat, J/(kg\cdot K) \\ C_t \\ C_t \\ total compression coefficient, 1/Pa \\ C_T \\ temperature correction coefficient \\ d_{hy} \\ hydraulic equivalent diameter, m \\ f \\ fiction coefficient \\ \phi \\ formation porosity \\ g \\ g \\ gravitational acceleration, m²/s \\ H \\ enthalpy, J/kg \\ h \\ thickness of the reservoir, m \\ \eta_s \\ separation efficiency \\ K \\ reservoir permeability, D \\ K(\alpha_g) \\ gas phase characteristic parameter \\ K_T \\ isothermal bulk elastic modulus, Pa \\ intermediate parameter \\ Nu \\ Nusselt number \\ p \\ wellbore pressure, Pa \\ p_{ave.f} \\ p_b \\ bottom hole pressure, Pa \\ p_e \\ reservoir permeability, Pa \\ wellhead backpressure, Pa \\ p_e \\ reservoir pressure, Pa \\ p_e \\ reservoir pressure, Pa \\ p_{norm} \\ wellbore pressure under normal condition, Pa \\ p_r \\ reservoir pressure, Pa \\ p_{norm} \\ wellbore pressure under normal condition, Pa \\ p_r \\ reservoir pressure, Pa \\ p_e \\ reservoir pressure, Pa \\ p_e \\ reservoir pressure under normal condition, Pa \\ p_r \\ reservoir pressure of the invading gas, K \\ reservoir pressure of the invading gas, K \\ reservoir temperature of the invading gas, K \\ reservoir temperature of the invading gas, K \\ reservoir temperature, ^{\circ}C $	-	•
$ \begin{array}{lll} C_{\rm p} & {\rm specific heat, } J/(kg\cdot K) \\ C_{\rm t} & {\rm total \ compression \ coefficient, } 1/Pa \\ C_{\rm T} & {\rm temperature \ correction \ coefficient} \\ d_{\rm hy} & {\rm hydraulic \ equivalent \ diameter, m} \\ f & {\rm friction \ coefficient} \\ \phi & {\rm formation \ porosity} \\ g & {\rm gravitational \ acceleration, m^2/s} \\ H & {\rm enthalpy, } J/kg \\ h & {\rm thickness \ of \ te \ reservoir, m} \\ \eta_s & {\rm separation \ efficiency} \\ K & {\rm reservoir \ permeability, D} \\ K(\alpha_g) & {\rm gas \ phase \ characteristic \ parameter} \\ K_{\rm T} & {\rm isothermal \ bulk \ elastic \ modulus, Pa} \\ A & {\rm intermediate \ parameter} \\ Nu & {\rm Nusselt \ number} \\ p & {\rm wellbore \ pressure, Pa} \\ p_{ave,f} & {\rm average \ pressure, Pa} \\ p_{b} & {\rm bottom \ hole \ pressure, Pa} \\ p_{e} & {\rm reservoir \ pressure, Pa} \\ p_{e} & {\rm wellhead \ backpressure, Pa} \\ p_{e} & {\rm wellhead \ backpressure, Pa} \\ p_{e} & {\rm reservoir \ pressure \ under \ normal \ condition, Pa} \\ p_{r} & {\rm mass \ flow \ rate, \ kg/(s\cdot m)} \\ Q_{e_{x}} & {\rm heat \ convection \ term \ between \ pas \ and \ drilling \ fluid, J} \\ p_{e} & {\rm reservoir \ temperature \ of \ the \ invading \ gas, K} \\ r_{e} & {\rm reservoir \ temperature \ of \ the \ invading \ gas, K} \\ r_{e} & {\rm reservoir \ temperature \ of \ the \ invading \ gas, K} \\ r_{e} & {\rm reservoir \ temperature \ of \ the \ invading \ gas, K} \\ r_{e} & {\rm reservoir \ temperature \ of \ the \ invading \ gas, K} \\ r_{e} & {\rm reservoir \ temperature \ of \ the \ invading \ gas, K} \\ r_{e} & {\rm reservoir \ temperature \ of \ the \ invading \ gas, K} \\ r_{e} & {\rm reservoir \ temperature \ of \ the \ invading \ gas, K} \\ r_{e} & {\rm reservoir \ temperature \ of \ the \ invading \ gas, K} \\ r_{e} & {\rm reservoir \ temperature \ of \ the \ invading \ gas, K} \\ r_{e} & {\rm reservoir \ temperature \ of \ the \ invading \ gas, K} \\ r_{e} & {\rm reservoir \ temperature \ of \ the \ invading \ gas, K} \\ r_{e} & {\rm reservoir \ temperature \ of \ the \ invading \ gas, K} \\ r_{e} & {\rm reservoir \ temperature \ of \ the \ invading $	-	•
$ \begin{array}{c} C_{\rm T} \\ C_{\rm T} $,	•
$ \begin{array}{lll} C_T & \text{temperature correction coefficient} \\ d_{\text{hy}} & \text{hydraulic equivalent diameter, m} \\ f & \text{friction coefficient} \\ \phi & \text{formation porosity} \\ g & \text{gravitational acceleration, m}^2/s \\ H & \text{enthalpy, J/kg} \\ h & \text{thickness of the reservoir, m} \\ \eta_5 & \text{separation efficiency} \\ K & \text{reservoir permeability, D} \\ K & \text{(α_g)} & \text{gas phase characteristic parameter} \\ K_T & \text{isothermal bulk elastic modulus, Pa} \\ A & \text{intermediate parameter} \\ Nu & \text{Nusselt number} \\ p & \text{wellbore pressure, Pa} \\ p_0 & \text{wellbore pressure, Pa} \\ p_0 & \text{wellhead backpressure, Pa} \\ p_0 & \text{wellhead backpressure, Pa} \\ p_0 & \text{reservoir pressure, Pa} \\ p_0 & \text{reservoir pressure, Pa} \\ p_0 & \text{maxs flow rate, kg/(s-m)} \\ Q_{\text{ex}} & \text{heat exchange term, J} \\ Q_{\text{conv}}^g & \text{heat convection term between gas and drilling fluid, J} \\ Q_{\text{conv}}^s & \text{heat convection term between hollow ball and drilling fluid Re} \\ Reynolds number & \text{average temperature of the invading gas, K} \\ T_e & \text{reservoir temperature of the invading gas, K} \\ T_e & \text{reservoir temperature of the invading gas, K} \\ T_{\text{or}} & \text{average temperature under normal condition, K} \\ T_p & \text{drilling fluid temperature under normal condition, K} \\ T_p & \text{drilling fluid temperature under normal condition, K} \\ T_p & \text{drilling fluid temperature under normal condition, K} \\ T_p & \text{drilling fluid temperature under normal condition, K} \\ T_p & \text{drilling fluid temperature under normal condition, K} \\ T_p & \text{drilling fluid temperature under normal condition, K} \\ T_p & \text{drilling fluid temperature under normal condition, K} \\ T_p & \text{drilling fluid temperature under normal condition, K} \\ T_p & \text{drilling fluid temperature under normal condition, K} \\ T_p & \text{drilling fluid temperature under normal condition, K} \\ T_p & \text{drilling fluid temperature under normal condition, K} \\ T_p & \text{drilling fluid temperature under normal condition, K} \\ T_p & \text{drilling fluid temperature under normal condition, K} \\ T_p & drilling fluid temperat$		
$\begin{array}{lll} d_{\rm hy} & {\rm hydraulic~equivalent~diameter,~m} \\ f & {\rm friction~coefficient} \\ \phi & {\rm formation~prosity} \\ g & {\rm gravitational~acceleration,~m}^2/s \\ H & {\rm enthalpy.~J/kg} \\ h & {\rm thickness~of~the~reservoir,~m} \\ \eta_{\rm S} & {\rm separation~efficiency} \\ K & {\rm reservoir~permeability,~D} \\ K\left(\alpha_{\rm g}\right) & {\rm gas~phase~characteristic~parameter} \\ K_{\rm T} & {\rm intermediate~parameter} \\ N_{\rm I} & {\rm Nusselt~number} \\ p & {\rm wellbore~pressure,~Pa} \\ p_{\rm aver,f} & {\rm average~pressure~of~the~invading~gas,~Pa} \\ p_{\rm b} & {\rm bottom~hole~pressure,~Pa} \\ p_{\rm e} & {\rm wellhead~backpressure,~Pa} \\ p_{\rm e} & {\rm wellhead~backpressure,~Pa} \\ p_{\rm e} & {\rm reservoir~pressure,~Pa} \\ p_{\rm e} & {\rm reservoir~pressure,~Pa} \\ p_{\rm e} & {\rm reservoir~pressure,~Pa} \\ p_{\rm e} & {\rm mass~flow~rate,~kg/(s\cdot m)} \\ q & {\rm mass~flow~rate,~kg/(s\cdot m)} \\ eat~convection~term~between~gas~and~drilling~fluid,~J} \\ q_{\rm e} & {\rm heat~convection~term~between~pas~and~drilling~fluid,~J} \\ q_{\rm e} & {\rm Reynolds~number} \\ q_{\rm aver,f} & {\rm average~temperature~of~the~invading~gas,~K} \\ T_{\rm e} & {\rm reservoir~temperature,~^{\circ}C} \\ T_{\rm in} & {\rm temperature~of~the~invading~gas,~K} \\ T_{\rm e} & {\rm reservoir~temperature,~^{\circ}C} \\ T_{\rm in} & {\rm temperature~of~the~invading~gas,~K} \\ T_{\rm p} & {\rm drilling~fluid~temperature~inside~the~drill~string,~K} \\ U & {\rm internal~energy,~J/kg} \\ v & {\rm velocity,~m/s} \\ v_{\rm e} & {\rm gas~silp~inte,~m/s} \\ v_{\rm e} & {\rm gas~compressibility~factor} \\ v_{\rm e} & {\rm gas~compres$		
friction coefficient φ formation porosity g gravitational acceleration, m^2/s H enthalpy, J/kg h thickness of the reservoir, m η_s separation efficiency K reservoir permeability, D K (α_g) gas phase characteristic parameter K reservoir permeability, D Nusselt number Nu Nusselt number p wellbore pressure, Pa Pave,f average pressure of the invading gas, Pa Pb bottom hole pressure, Pa Pc wellhead backpressure, Pa Pc wellhead backpressure, Pa Pc wellbore pressure under normal condition, Pa Pr Prandtl number q mass flow rate, $kg/(s \cdot m)$ Qex heat exchange term, J Nea convection term between gas and drilling fluid, J Qex heat convection term between hollow ball and drilling fluid Re Reynolds number Tave,f average temperature of the invading gas, K reservoir temperature, °C Tin temperature of the injected drilling fluid, K Tre temperature of the injected drilling fluid, K Tre average temperature under normal condition, K drilling fluid temperature inside the drill string, K U internal energy, J/kg V velocity, m/s Z gas compressibility factor Ze gas compressibility factor ze gas compressibility factor under reservoir environment β_T thermal expansion coefficient of the pore fluid, K-1 decreasing term Δ roughness of the pipe wall θ well inclination angle, rad λ thermal conductivity, $W/(m \cdot K)$ Viscosity, $P_a \cdot s$ θ density, kg/m^3 Subscript g gas I drilling fluid S hollow ball m gas-liquid-solid mixed fluid f formation	.*	•
$ \begin{array}{cccccccccccccccccccccccccccccccccccc$		•
$\begin{array}{lll} g & & & & & & \\ H & & & & & \\ h & & & & & \\ h & & & & \\ h & & & &$		
$ H \\ h \\ h \\ thickness of the reservoir, m \\ η_s \\ separation efficiency \\ K \\ reservoir permeability, D \\ K (α_g) \\ gas phase characteristic parameter \\ K_T \\ isothermal bulk elastic modulus, Pa \\ A \\ intermediate parameter \\ Nu \\ Nusselt number \\ p \\ wellbore pressure, Pa \\ p_{ave,f} \\ average pressure of the invading gas, Pa \\ p_b \\ bottom hole pressure, Pa \\ p_c \\ wellhead backpressure, Pa \\ p_e \\ reservoir pressure, Pa \\ p_e \\ reservoir pressure, Pa \\ p_{norm} \\ wellbore pressure under normal condition, Pa \\ p_r \\ Prandtl number \\ q \\ mass flow rate, kg/(s·m) \\ heat exchange term, J \\ Q_{con}^g \\ heat exchange term, J \\ Q_{con}^g \\ heat convection term between gas and drilling fluid, J \\ P_{conv} \\ heat convection term between hollow ball and drilling fluid \\ Re \\ Reynolds number \\ T_{ave,f} \\ average temperature of the invading gas, K \\ T_e \\ reservoir temperature, "C \\ T_{in} \\ temperature of the injected drilling fluid, K \\ T_{norm} \\ wellbore temperature under normal condition, K \\ T_{p} \\ drilling fluid temperature inside the drill string, K \\ U \\ internal energy, J/kg \\ v \\ velocity, m/s \\ v_{co} \\ gas slip rate, m/s \\ v_{c} \\ gas compressibility factor under reservoir environment \\ H_{T} \\ thermal expansion coefficient of the pore fluid, K^{-1} \\ decreasing term \\ \Delta \\ roughness of the pipe wall \\ \theta \\ well inclination angle, rad \\ hermal conductivity, W/(m·K) \\ \mu \\ viscosity, P_{a} \cdot s \\ density, kg/m^3 \\ Subscript \\ g \\ gas \\ I \\ drilling fluid \\ s \\ hollow ball \\ m \\ gas-liquid-solid mixed fluid \\ f \\ formation \\$	•	
h thickness of the reservoir, m η _S separation efficiency K reservoir permeability, D K (α_g) gas phase characteristic parameter K_T isothermal bulk elastic modulus, Pa M intermediate parameter Nu Nusselt number p wellbore pressure, Pa p wellbore pressure, Pa p wellhead backpressure, Pa p wellhead backpressure, Pa p reservoir pressure, Pa p wellhoad backpressure, Pa p reservoir pressure, Pa p wellbore pressure under normal condition, Pa p reservoir pressure, Pa p re		
$\begin{array}{lll} \eta_{\rm S} & {\rm separation efficiency} \\ K & {\rm reservoir permeability, D} \\ K \left(\alpha_{\rm g}\right) & {\rm gas phase characteristic parameter} \\ K_{\rm T} & {\rm isothermal bulk elastic modulus, Pa} \\ A & {\rm intermediate parameter} \\ Nu & {\rm Nusselt number} \\ p & {\rm wellbore pressure, Pa} \\ p_{\rm ave,f} & {\rm average pressure of the invading gas, Pa} \\ p_{\rm b} & {\rm bottom hole pressure, Pa} \\ p_{\rm c} & {\rm wellhead backpressure, Pa} \\ p_{\rm c} & {\rm wellhead backpressure, Pa} \\ p_{\rm e} & {\rm reservoir pressure, Pa} \\ p_{\rm e} & {\rm reservoir pressure, pa} \\ p_{\rm e} & {\rm mass flow rate, kg/(s \cdot m)} \\ Q_{\rm ex} & {\rm heat exchange term, J} \\ Q_{\rm conv}^{\rm g} & {\rm heat exchange term, J} \\ Q_{\rm conv}^{\rm g} & {\rm heat convection term between gas and drilling fluid, J} \\ Q_{\rm conv}^{\rm e} & {\rm heat convection term between hollow ball and drilling fluid} \\ Re & {\rm Reynolds number} \\ T_{\rm ave,f} & {\rm average temperature of the invading gas, K} \\ T_{\rm e} & {\rm reservoir temperature} \\ T_{\rm in} & {\rm temperature of the injected drilling fluid, K} \\ T_{\rm norm} & {\rm wellbore temperature under normal condition, K} \\ T_{\rm p} & {\rm drilling fluid temperature inside the drill string, K} \\ U & {\rm internal energy, J/kg} \\ v & {\rm velocity, m/s} \\ v_{\infty} & {\rm gas slip rate, m/s} \\ v_{\rm c} & {\rm gas compressibility factor} \\ z_{\rm e} & {\rm gas compressibility factor} \\ z_{\rm e} & {\rm gas compressibility factor under reservoir environment} \\ \theta_{\rm T} & {\rm thermal expansion coefficient of the pore fluid, K^{-1}} \\ decreasing term \\ \Delta & {\rm thermal conductivity, W/(m \cdot K)} \\ \mu & {\rm viscosity, Pa \cdot s} \\ \rho & {\rm density, kg/m^3} \\ {\rm Subscript} \\ g & {\rm gas} \\ 1 & {\rm drilling fluid} \\ {\rm s} & {\rm hollow ball} \\ {\rm m} & {\rm gas -liquid-solid mixed fluid} \\ {\rm f} & {\rm formation} \\ \end{array}$		10.0.0
$ \begin{array}{c} K \\ K \\ (\alpha_g) \\ gas phase characteristic parameter \\ K_T \\ isothermal bulk elastic modulus, Pa \\ A \\ intermediate parameter \\ Nu \\ Nusselt number \\ p \\ wellbore pressure, Pa \\ p_{ave,f} \\ average pressure of the invading gas, Pa \\ p_b \\ bottom hole pressure, Pa \\ p_c \\ wellhead backpressure, Pa \\ p_e \\ reservoir pressure, Pa \\ p_{norm} \\ wellbore pressure under normal condition, Pa \\ p_T \\ Pr \\ Prandtl number \\ q \\ mass flow rate, kg/(s \cdot m) \\ heat convection term between gas and drilling fluid, J \\ Q_{\infty}^{e} \\ conv \\ heat convection term between hollow ball and drilling fluid \\ Re \\ Reynolds number \\ T_{ave,f} \\ T_{e} \\ reservoir temperature of the invading gas, K \\ T_{e} \\ reservoir temperature of the injected drilling fluid, K \\ T_{norm} \\ wellbore temperature under normal condition, K \\ T_{p} \\ drilling fluid temperature inside the drill string, K \\ U \\ internal energy, J/kg \\ v \\ velocity, m/s \\ v_{\infty} \\ gas sharacteristic velocity, m/s \\ z \\ gas compressibility factor under reservoir environment \\ k_T \\ thermal expansion coefficient of the pore fluid, K^{-1} \\ decreasing term \\ \Delta \\ roughness of the pipe wall \\ \theta \\ well inclination angle, rad \\ \lambda \\ thermal conductivity, W/(m \cdot K) \\ viscosity, Pa \cdot s \\ \rho \\ density, kg/m^3 \\ Subscript \\ g \\ gas \\ 1 \\ drilling fluid \\ s \\ hollow ball \\ m \\ gas-liquid-solid mixed fluid \\ f \\ formation \\ \end{cases}$		
$ \begin{array}{lll} K(\alpha_g) & \text{gas phase characteristic parameter} \\ K_T & \text{isothermal bulk elastic modulus, Pa} \\ A & \text{intermediate parameter} \\ Nu & \text{Nusselt number} \\ p & \text{wellbore pressure, Pa} \\ p_{ave,f} & \text{average pressure of the invading gas, Pa} \\ p_b & \text{bottom hole pressure, Pa} \\ p_c & \text{wellhead backpressure, Pa} \\ p_e & \text{reservoir pressure, Pa} \\ p_e & \text{reservoir pressure under normal condition, Pa} \\ p_T & \text{Prandtl number} \\ q & \text{mass flow rate, } kg/(s \cdot m) \\ Q_{ex} & \text{heat exchange term, J} \\ Q_{conv}^g & \text{heat convection term between gas and drilling fluid, J} \\ Q_{conv}^s & \text{heat convection term between hollow ball and drilling fluid } \\ Re & \text{Reynolds number} \\ T_{ave,f} & \text{average temperature of the invading gas, K} \\ T_e & \text{reservoir temperature of the injected drilling fluid, K} \\ T_norm & \text{wellbore temperature under normal condition, K} \\ T_p & \text{drilling fluid temperature inside the drill string, K} \\ U & \text{internal energy, } J/kg \\ v & \text{velocity, } m/s \\ v_c & \text{gas slip rate, } m/s \\ v_c & \text{gas compressibility factor} \\ z_e & \text{gas compressibility factor} \\ z_e & \text{gas compressibility factor under reservoir environment} \\ \theta_T & \text{thermal expansion coefficient of the pore fluid, } K^{-1} \\ \phi & \text{decreasing term} \\ \Delta & \text{toughness of the pipe wall} \\ \theta & \text{well inclination angle, rad} \\ \lambda & \text{thermal conductivity, } W/(m \cdot K) \\ \mu & \text{viscosity, } Pa \cdot s \\ \rho_{p} & \text{density, } kg/m^3 \\ Subscript \\ g & \text{gas} \\ 1 & \text{drilling fluid} \\ \text{s} & \text{hollow ball} \\ \text{m} & \text{gas-liquid-solid mixed fluid} \\ \text{f} & \text{formation} \end{array}$		•
$ \begin{array}{llllllllllllllllllllllllllllllllllll$		
A intermediate parameter Nu Nusselt number p wellbore pressure, Pa $p_{ave,f}$ average pressure of the invading gas, Pa p_b bottom hole pressure, Pa p_c wellhead backpressure, Pa p_c wellhead backpressure, Pa p_c wellbore pressure under normal condition, Pa p_r Prandtl number q mass flow rate, $kg/(s \cdot m)$ Q_{ex} heat exchange term, J Q_{ex} heat convection term between gas and drilling fluid, J Q_{ex} heat convection term between hollow ball and drilling fluid Re Reynolds number $T_{ave,f}$ average temperature of the invading gas, K T_e reservoir temperature, °C T_{in} temperature of the injected drilling fluid, K T_{norm} wellbore temperature under normal condition, K T_{p} drilling fluid temperature inside the drill string, K U internal energy, J/kg v velocity, m/s z gas slip rate, m/s v_c gas compressibility factor z gas compressibility factor under reservoir environment t thermal expansion coefficient of the pore fluid, K $^{-1}$ γ decreasing term Δ roughness of the pipe wall θ well inclination angle, rad t thermal conductivity, $W/(m \cdot K)$ μ viscosity, $P_a \cdot s$ ρ density, kg/m^3 Subscriptgas g gas t t		
NuNusselt number p wellbore pressure, Pa $p_{ave,f}$ average pressure of the invading gas, Pa p_b bottom hole pressure, Pa p_c wellhead backpressure, Pa p_e reservoir pressure, Pa p_nonm wellbore pressure under normal condition, Pa p_r Prandtl number q mass flow rate, kg/(s·m) Q_{ex} heat exchange term, J Q_{conv} heat convection term between gas and drilling fluid, J p_{conv} heat convection term between hollow ball and drilling fluid p_{conv} heat convection term between hollow ball and drilling fluid p_{conv} heat convection term between hollow ball and drilling fluid p_{conv} heat convection term between hollow ball and drilling fluid p_{conv} heat convection term between hollow ball and drilling fluid, K p_{conv} temperature of the injected drilling fluid, K p_{conv} temperature of the injected drilling fluid, K p_{conv} wellbore temperature under normal condition, K p_{conv} drilling fluid temperature inside the drill string, K p_{conv} under temperature inside the drill string, K p_{conv} velocity, m/s p_{conv} gas characteristic velocity, m/s p_{conv} gas compressibility factor under reservoir environment p_{conv} thermal expansion coefficient of the pore fluid, K^-1 p_{conv} decreasing term p_{conv} density, kg/m³Subscriptgas p_{conv} de	•	·
$\begin{array}{lll} p & \text{wellbore pressure, Pa} \\ p_{ave,f} & \text{average pressure of the invading gas, Pa} \\ p_b & \text{bottom hole pressure, Pa} \\ p_c & \text{wellhead backpressure, Pa} \\ p_c & \text{reservoir pressure, Pa} \\ p_e & \text{reservoir pressure, Pa} \\ p_{\text{norm}} & \text{wellbore pressure under normal condition, Pa} \\ Pr & \text{Prandtl number} \\ q & \text{mass flow rate, kg/(s \cdot m)} \\ Q_{ex} & \text{heat exchange term, J} \\ Q_{s}^{g} & \text{conv} & \text{heat convection term between gas and drilling fluid, J} \\ Q_{c \text{conv}}^{g} & \text{heat convection term between hollow ball and drilling fluid} \\ Re & \text{Reynolds number} \\ T_{ave,f} & \text{average temperature of the invading gas, K} \\ T_{e} & \text{reservoir temperature, }^{\circ}C \\ T_{in} & \text{temperature of the injected drilling fluid, K} \\ T_{norm} & \text{wellbore temperature under normal condition, K} \\ T_{p} & \text{drilling fluid temperature inside the drill string, K} \\ U & \text{internal energy, J/kg} \\ v & \text{velocity, m/s} \\ v_{\infty} & \text{gas slip rate, m/s} \\ v_{c} & \text{gas compressibility factor} \\ z_{e} & \text{gas compressibility factor} \\ z_{e} & \text{gas compressibility factor under reservoir environment} \\ \beta_{T} & \text{thermal expansion coefficient of the pore fluid, K}^{-1} \\ decreasing term \\ \Delta & \text{roughness of the pipe wall} \\ \theta & \text{well inclination angle, rad} \\ \lambda & \text{thermal conductivity, W/(m·K)} \\ \mu & \text{viscosity, Pa·s} \\ \rho & \text{density, kg/m}^{3} \\ \text{Subscript} \\ g & \text{gas} \\ 1 & \text{drilling fluid} \\ \text{solution bollow ball} \\ m & \text{gas-liquid-solid mixed fluid} \\ f & \text{formation} \\ \end{array}$		•
$\begin{array}{lll} p_{\rm ave,f} & {\rm average\ pressure\ of\ the\ invading\ gas,\ Pa} \\ p_{\rm b} & {\rm bottom\ hole\ pressure,\ Pa} \\ p_{\rm c} & {\rm wellhead\ backpressure,\ Pa} \\ p_{\rm c} & {\rm wellhead\ backpressure,\ Pa} \\ p_{\rm e} & {\rm reservoir\ pressure,\ Pa} \\ p_{\rm norm} & {\rm wellbore\ pressure\ under\ normal\ condition,\ Pa} \\ p_{\rm r} & {\rm Prandtl\ number} \\ q & {\rm mass\ flow\ rate,\ kg/(s\cdot m)} \\ Q_{\rm ex} & {\rm heat\ exchange\ term,\ J} \\ Q_{\rm ex} & {\rm heat\ convection\ term\ between\ gas\ and\ drilling\ fluid,\ J} \\ Q_{\rm exconv} & {\rm heat\ convection\ term\ between\ hollow\ ball\ and\ drilling\ fluid\ Re\ Reynolds\ number} \\ T_{\rm ave,f} & {\rm average\ temperature\ of\ the\ invading\ gas,\ K} \\ T_{\rm e} & {\rm reservoir\ temperature\ of\ the\ invading\ gas,\ K} \\ T_{\rm e} & {\rm reservoir\ temperature\ of\ the\ invading\ gas,\ K} \\ T_{\rm e} & {\rm reservoir\ temperature\ of\ the\ invading\ gas,\ K} \\ T_{\rm e} & {\rm reservoir\ temperature\ of\ the\ invading\ gas,\ K} \\ T_{\rm e} & {\rm reservoir\ temperature\ of\ the\ invading\ gas,\ K} \\ T_{\rm e} & {\rm reservoir\ temperature\ of\ the\ invading\ gas,\ K} \\ T_{\rm e} & {\rm reservoir\ temperature\ of\ the\ invading\ gas,\ K} \\ T_{\rm e} & {\rm reservoir\ temperature\ of\ the\ injected\ drilling\ fluid,\ K} \\ T_{\rm norm} & {\rm wellbore\ temperature\ under\ normal\ condition,\ K} \\ T_{\rm p} & {\rm drilling\ fluid\ temperature\ inside\ the\ drill\ string,\ K} \\ V & {\rm velocity,\ m/s} \\ V_{\infty} & {\rm gas\ slip\ rate,\ m/s} \\ V_{\infty} & {\rm gas\ compressibility\ factor} \\ Z_{\rm e} & {\rm gas\ compressibility\ factor\ under\ reservoir\ environment} \\ D_{\rm o} & {\rm velocity,\ pa-s} \\ D_{\rm o} & {\rm density,\ pa-s} \\ D_{\rm o} & {\rm density,\ kg/m}^3 \\ Subscript \\ g & {\rm gas} \\ 1 & {\rm drilling\ fluid} \\ {\rm s} & {\rm hollow\ ball} \\ {\rm m} & {\rm gas-liquid-solid\ mixed\ fluid} \\ f & {\rm formation} \\ \end{array}$		
$\begin{array}{lll} p_{\rm b} & {\rm bottom\ hole\ pressure,\ Pa} \\ p_{\rm c} & {\rm wellhead\ backpressure,\ Pa} \\ p_{\rm c} & {\rm wellhead\ backpressure,\ Pa} \\ p_{\rm e} & {\rm reservoir\ pressure,\ Pa} \\ p_{\rm e} & {\rm reservoir\ pressure,\ Pa} \\ p_{\rm horm} & {\rm wellbore\ pressure\ under\ normal\ condition,\ Pa} \\ Pr & {\rm Prandtl\ number} \\ q & {\rm mass\ flow\ rate,\ kg/(s\cdot m)} \\ Q_{\rm ex} & {\rm heat\ exchange\ term,\ J} \\ Q_{\rm ex}^{\rm c} & {\rm heat\ exchange\ term,\ J} \\ Q_{\rm ex}^{\rm c} & {\rm heat\ exchange\ term,\ J} \\ Q_{\rm ex}^{\rm c} & {\rm heat\ exchange\ term,\ J} \\ Q_{\rm ex}^{\rm c} & {\rm heat\ exchange\ term,\ J} \\ Q_{\rm ex}^{\rm c} & {\rm heat\ exchange\ term,\ J} \\ Q_{\rm ex}^{\rm c} & {\rm heat\ exchange\ term,\ J} \\ Q_{\rm ex}^{\rm c} & {\rm heat\ exchange\ term,\ J} \\ Q_{\rm ex}^{\rm c} & {\rm heat\ exchange\ term,\ J} \\ Q_{\rm ex}^{\rm c} & {\rm heat\ exchange\ term,\ J} \\ Q_{\rm ex}^{\rm c} & {\rm heat\ exchange\ term,\ J} \\ R_{\rm e} & {\rm Reynolds\ number} \\ T_{\rm ave,f} & {\rm average\ temperature\ of\ the\ invading\ gas,\ K} \\ T_{\rm e} & {\rm reservoir\ temperature\ of\ the\ invading\ gas,\ K} \\ T_{\rm e} & {\rm reservoir\ temperature\ of\ the\ invading\ gas,\ K} \\ T_{\rm e} & {\rm reservoir\ temperature\ of\ the\ invading\ gas,\ K} \\ T_{\rm norm} & {\rm wellbore\ temperature\ of\ the\ invading\ gas,\ K} \\ T_{\rm norm} & {\rm wellbore\ temperature\ of\ the\ invading\ gas,\ K} \\ T_{\rm norm} & {\rm wellbore\ temperature\ of\ the\ invading\ gas,\ K} \\ T_{\rm norm} & {\rm wellbore\ temperature\ of\ the\ invading\ gas,\ K} \\ T_{\rm norm} & {\rm wellbore\ temperature\ of\ the\ invading\ gas,\ K} \\ T_{\rm norm} & {\rm wellbore\ temperature\ of\ the\ invading\ gas,\ K} \\ T_{\rm norm} & {\rm wellbore\ temperature\ of\ the\ invading\ gas,\ K} \\ T_{\rm norm} & {\rm wellbore\ temperature\ of\ the\ invading\ gas,\ K} \\ T_{\rm norm} & {\rm wellbore\ temperature\ of\ the\ invading\ gas,\ K} \\ T_{\rm norm} & {\rm wellbore\ temperature\ of\ the\ invading\ gas,\ K} \\ T_{\rm norm} & {\rm wellbore\ temperature\ of\ the\ invading\ gas,\ K} \\ T_{\rm norm} & {\rm vollow} & $	•	•
$\begin{array}{llll} p_{c} & \text{wellhead backpressure, Pa} \\ p_{e} & \text{reservoir pressure, Pa} \\ p_{born} & \text{wellbore pressure under normal condition, Pa} \\ Pr & \text{Prandtl number} \\ q & \text{mass flow rate, kg/(s \cdot m)} \\ Q_{ex} & \text{heat exchange term, J} \\ Q_{conv}^{g} & \text{heat convection term between gas and drilling fluid, J} \\ Q_{conv}^{g} & \text{heat convection term between hollow ball and drilling fluid} \\ Re & \text{Reynolds number} \\ T_{ave,f} & \text{average temperature of the invading gas, K} \\ T_{e} & \text{reservoir temperature, } ^{\circ}{C} \\ T_{in} & \text{temperature of the injected drilling fluid, K} \\ T_{norm} & \text{wellbore temperature under normal condition, K} \\ T_{p} & \text{drilling fluid temperature inside the drill string, K} \\ U & \text{internal energy, J/kg} \\ v & \text{velocity, m/s} \\ v_{\infty} & \text{gas slip rate, m/s} \\ v_{c} & \text{gas compressibility factor} \\ z_{e} & \text{gas compressibility factor} \\ z_{e} & \text{gas compressibility factor under reservoir environment} \\ \beta_{T} & \text{thermal expansion coefficient of the pore fluid, K}^{-1} \\ \phi & \text{decreasing term} \\ \Delta & \text{roughness of the pipe wall} \\ \theta & \text{well inclination angle, rad} \\ \lambda & \text{thermal conductivity, W/(m·K)} \\ \mu & \text{viscosity, Pa·s} \\ \rho & \text{density, kg/m}^{3} \\ \text{Subscript} \\ g & \text{gas} \\ 1 & \text{drilling fluid} \\ \text{s} & \text{hollow ball} \\ \text{m} & \text{gas-liquid-solid mixed fluid} \\ f & \text{formation} \\ \end{array}$		
$\begin{array}{lll} p_{\text{e}} & \text{reservoir pressure, Pa} \\ p_{\text{norm}} & \text{wellbore pressure under normal condition, Pa} \\ Pr & \text{Prandtl number} \\ q & \text{mass flow rate, kg/(s \cdot m)} \\ Q_{\text{ex}} & \text{heat exchange term, J} \\ Q_{\text{conv}}^{\text{c}} & \text{heat convection term between gas and drilling fluid, J} \\ Q_{\text{conv}}^{\text{c}} & \text{heat convection term between hollow ball and drilling fluid} \\ Re & \text{Reynolds number} \\ T_{\text{ave,f}} & \text{average temperature of the invading gas, K} \\ T_{\text{e}} & \text{reservoir temperature, }^{\circ}\text{C} \\ T_{\text{in}} & \text{temperature of the injected drilling fluid, K} \\ T_{\text{norm}} & \text{wellbore temperature under normal condition, K} \\ T_{\text{p}} & \text{drilling fluid temperature inside the drill string, K} \\ U & \text{internal energy, J/kg} \\ v & \text{velocity, m/s} \\ v_{\infty} & \text{gas slip rate, m/s} \\ v_{\text{c}} & \text{gas compressibility factor} \\ z_{\text{e}} & \text{gas compressibility factor under reservoir environment} \\ \beta_{\text{T}} & \text{thermal expansion coefficient of the pore fluid, K}^{-1} \\ \phi & \text{decreasing term} \\ \Delta & \text{roughness of the pipe wall} \\ \theta & \text{well inclination angle, rad} \\ \lambda & \text{thermal conductivity, W/(m·K)} \\ \mu & \text{viscosity, Pa·s} \\ \rho & \text{density, kg/m}^3 \\ \text{Subscript} \\ g & \text{gas} \\ 1 & \text{drilling fluid} \\ \text{s} & \text{hollow ball} \\ \text{m} & \text{gas-liquid-solid mixed fluid} \\ \text{f} & \text{formation} \end{array}$		•
$\begin{array}{lll} p_{\text{norm}} & \text{wellbore pressure under normal condition, Pa} \\ Pr & \text{Prandtl number} \\ q & \text{mass flow rate, kg/(s·m)} \\ Q_{\text{ex}} & \text{heat exchange term, J} \\ Q_{\text{conv}}^{\text{g}} & \text{heat convection term between gas and drilling fluid, J} \\ Q_{\text{conv}}^{\text{g}} & \text{heat convection term between hollow ball and drilling fluid} \\ Re & \text{Reynolds number} \\ T_{\text{ave,f}} & \text{average temperature of the invading gas, K} \\ T_{\text{e}} & \text{reservoir temperature} ^{\circ}\text{C} \\ T_{\text{in}} & \text{temperature of the injected drilling fluid, K} \\ T_{\text{norm}} & \text{wellbore temperature under normal condition, K} \\ T_{\text{p}} & \text{drilling fluid temperature inside the drill string, K} \\ U & \text{internal energy, J/kg} \\ v & \text{velocity, m/s} \\ v_{\infty} & \text{gas slip rate, m/s} \\ v_{\text{c}} & \text{gas compressibility factor} \\ z_{\text{e}} & \text{gas compressibility factor} \\ z_{\text{e}} & \text{gas compressibility factor under reservoir environment} \\ \theta_{\text{T}} & \text{thermal expansion coefficient of the pore fluid, K}^{-1} \\ \gamma & \text{decreasing term} \\ \Delta & \text{roughness of the pipe wall} \\ \theta & \text{well inclination angle, rad} \\ \lambda & \text{thermal conductivity, W/(m·K)} \\ v_{\text{iscosity, Pa·s}} & \text{density, kg/m}^3 \\ \text{Subscript} \\ g & \text{gas} \\ 1 & \text{drilling fluid} \\ \text{s} & \text{hollow ball} \\ \text{m} & \text{gas-liquid-solid mixed fluid} \\ f & \text{formation} \\ \end{array}$		
Pr Prandtl number q mass flow rate, kg/(s·m) Q_{ex} heat exchange term, J Q_{conv} heat convection term between gas and drilling fluid, J Q_{conv}^{g} heat convection term between hollow ball and drilling fluid Re Reynolds number $T_{ave,f}$ average temperature of the invading gas, K T_{e} reservoir temperature, °C T_{in} temperature of the injected drilling fluid, K T_{norm} wellbore temperature under normal condition, K T_{p} drilling fluid temperature inside the drill string, K U internal energy, J/kg v velocity, m/s v_{co} gas slip rate, m/s v_{c} gas characteristic velocity, m/s z gas compressibility factor z_{e} gas compressibility factor under reservoir environment ϕ thermal expansion coefficient of the pore fluid, K $^{-1}$ ϕ decreasing term ϕ well inclination angle, rad ϕ thermal conductivity, W/(m·K) ϕ viscosity, $P_{a} \cdot s$ ϕ density, $P_{a} \cdot s$ <td></td> <td>•</td>		•
$\begin{array}{lll} q & \text{mass flow rate, kg/(s\cdot m)} \\ Q_{\text{ex}} & \text{heat exchange term, J} \\ Q_{\text{conv}}^{\text{g}} & \text{heat convection term between gas and drilling fluid, J} \\ Q_{\text{conv}}^{\text{g}} & \text{heat convection term between hollow ball and drilling fluid} \\ Re & \text{Reynolds number} \\ T_{\text{ave,f}} & \text{average temperature of the invading gas, K} \\ T_{\text{e}} & \text{reservoir temperature, }^{\circ}\text{C} \\ T_{\text{in}} & \text{temperature of the injected drilling fluid, K} \\ T_{\text{norm}} & \text{wellbore temperature under normal condition, K} \\ T_{p} & \text{drilling fluid temperature inside the drill string, K} \\ U & \text{internal energy, J/kg} \\ v & \text{velocity, m/s} \\ v_{\infty} & \text{gas slip rate, m/s} \\ v_{\text{c}} & \text{gas compressibility factor} \\ z_{\text{e}} & \text{gas compressibility factor} \\ z_{\text{e}} & \text{gas compressibility factor under reservoir environment} \\ \beta_{\text{T}} & \text{thermal expansion coefficient of the pore fluid, K}^{-1} \\ \gamma & \text{decreasing term} \\ \Delta & \text{roughness of the pipe wall} \\ \theta & \text{well inclination angle, rad} \\ \lambda & \text{thermal conductivity, W/(m·K)} \\ \mu & \text{viscosity, Pa·s} \\ \rho & \text{density, Pa·s} \\ \text{density, Pg/m}^{3} \\ \text{Subscript} \\ \text{g} & \text{gas} \\ 1 & \text{drilling fluid} \\ \text{s} & \text{hollow ball} \\ \text{m} & \text{gas-liquid-solid mixed fluid} \\ \text{f} & \text{formation} \\ \end{array}$	-	•
$\begin{array}{lll} Q_{\rm ex}^{\rm x} & {\rm heat\ exchange\ term,\ J} \\ Q_{\rm conv}^{\rm g} & {\rm heat\ convection\ term\ between\ gas\ and\ drilling\ fluid,\ J} \\ Q_{\rm conv}^{\rm g} & {\rm heat\ convection\ term\ between\ gas\ and\ drilling\ fluid,\ J} \\ Q_{\rm conv}^{\rm g} & {\rm heat\ convection\ term\ between\ hollow\ ball\ and\ drilling\ fluid\ Re} \\ Re & {\rm Reynolds\ number} \\ T_{\rm ave,f} & {\rm average\ temperature\ of\ the\ invading\ gas,\ K} \\ T_{\rm e} & {\rm reservoir\ temperature\ of\ the\ invading\ gas,\ K} \\ T_{\rm e} & {\rm reservoir\ temperature\ of\ the\ invading\ gas,\ K} \\ T_{\rm e} & {\rm temperature\ of\ the\ injected\ drilling\ fluid,\ K} \\ T_{\rm norm} & {\rm wellbore\ temperature\ under\ normal\ condition,\ K} \\ T_{\rm p} & {\rm drilling\ fluid\ temperature\ inside\ the\ drill\ string,\ K} \\ U & {\rm internal\ energy,\ J/kg} \\ v & {\rm velocity,\ m/s} \\ v_{\rm o} & {\rm gas\ slip\ rate,\ m/s} \\ v_{\rm c} & {\rm gas\ compressibility\ factor} \\ z_{\rm e} & {\rm gas\ compressibility\ factor\ under\ reservoir\ environment} \\ t_{\rm hermal\ expansion\ coefficient\ of\ the\ pore\ fluid,\ K^{-1}} \\ \psi & {\rm decreasing\ term} \\ \Delta & {\rm roughness\ of\ the\ pipe\ wall} \\ \theta & {\rm well\ inclination\ angle,\ rad} \\ \lambda & {\rm thermal\ conductivity,\ W/(m\cdot K)} \\ \mu & {\rm viscosity,\ Pa\cdot s} \\ \rho & {\rm density,\ kg/m^3} \\ Subscript \\ g & {\rm gas} \\ 1 & {\rm drilling\ fluid\ s} \\ s & {\rm hollow\ ball} \\ m & {\rm gas-liquid-solid\ mixed\ fluid} \\ f & {\rm formation} \end{array}$		
$\begin{array}{lll} Q_{\text{conv}}^{\text{W}} & \text{heat convection term between gas and drilling fluid, J} \\ Q_{\text{conv}}^{\text{S}} & \text{heat convection term between hollow ball and drilling fluid} \\ Re & \text{Reynolds number} \\ T_{\text{ave,f}} & \text{average temperature of the invading gas, K} \\ T_{\text{e}} & \text{reservoir temperature, }^{\circ}\text{C} \\ T_{\text{in}} & \text{temperature of the injected drilling fluid, K} \\ T_{\text{norm}} & \text{wellbore temperature under normal condition, K} \\ T_{\text{p}} & \text{drilling fluid temperature inside the drill string, K} \\ U & \text{internal energy, J/kg} \\ v & \text{velocity, m/s} \\ v_{\infty} & \text{gas slip rate, m/s} \\ v_{\text{c}} & \text{gas compressibility factor} \\ z_{\text{e}} & \text{gas compressibility factor under reservoir environment} \\ \beta_{\text{T}} & \text{thermal expansion coefficient of the pore fluid, K}^{-1} \\ \phi & \text{decreasing term} \\ \Delta & \text{roughness of the pipe wall} \\ \theta & \text{well inclination angle, rad} \\ \lambda & \text{thermal conductivity, W/(m·K)} \\ \mu & \text{viscosity, Pa·s} \\ \rho & \text{density, kg/m}^3 \\ \text{Subscript} \\ g & \text{gas} \\ 1 & \text{drilling fluid} \\ \text{s} & \text{hollow ball} \\ \text{m} & \text{gas-liquid-solid mixed fluid} \\ \text{f} & \text{formation} \end{array}$		
$\begin{array}{lll} Q_{\text{conv}}^{\text{c}} & \text{heat convection term between hollow ball and drilling fluid} \\ Re & \text{Reynolds number} \\ T_{\text{ave,f}} & \text{average temperature of the invading gas, K} \\ T_{\text{e}} & \text{reservoir temperature, }^{\circ}\text{C} \\ T_{\text{in}} & \text{temperature of the injected drilling fluid, K} \\ T_{\text{norm}} & \text{wellbore temperature under normal condition, K} \\ Wellbore temperature under normal condition, K} \\ U & \text{internal energy, J/kg} \\ V & \text{velocity, m/s} \\ V_{\infty} & \text{gas slip rate, m/s} \\ V_{\text{c}} & \text{gas characteristic velocity, m/s} \\ z & \text{gas compressibility factor} \\ z_{\text{e}} & \text{gas compressibility factor under reservoir environment} \\ \beta_{\text{T}} & \text{thermal expansion coefficient of the pore fluid, K}^{-1} \\ \gamma & \text{decreasing term} \\ \Delta & \text{roughness of the pipe wall} \\ \theta & \text{well inclination angle, rad} \\ \lambda & \text{thermal conductivity, W/(m \cdot \text{K})} \\ \mu & \text{viscosity, Pa \cdot s} \\ \rho & \text{density, kg/m}^3 \\ \text{Subscript} \\ g & \text{gas} \\ 1 & \text{drilling fluid} \\ \text{s} & \text{hollow ball} \\ \text{m} & \text{gas-liquid-solid mixed fluid} \\ f & \text{formation} \\ \end{array}$		
ReReynolds number $T_{ave,f}$ average temperature of the invading gas, K T_e reservoir temperature, °C T_{in} temperature of the injected drilling fluid, K T_{norm} wellbore temperature under normal condition, K T_{p} drilling fluid temperature inside the drill string, K U internal energy, J/kg v velocity, m/s v_c gas slip rate, m/s v_c gas characteristic velocity, m/s z gas compressibility factor z_e gas compressibility factor under reservoir environment β_T thermal expansion coefficient of the pore fluid, K $^{-1}$ γ decreasing term Δ roughness of the pipe wall θ well inclination angle, rad λ thermal conductivity, W/(m·K) μ viscosity, Pa·s·s ρ density, kg/m 3 Subscriptgasggas1drilling fluidshollow ballmgas-liquid-solid mixed fluidfformation		
$\begin{array}{lll} T_{\rm ave,f} & {\rm average\ temperature\ of\ the\ invading\ gas,\ K} \\ T_{\rm e} & {\rm reservoir\ temperature,\ ^{\circ}C} \\ T_{\rm in} & {\rm temperature\ of\ the\ injected\ drilling\ fluid,\ K} \\ T_{\rm norm} & {\rm wellbore\ temperature\ under\ normal\ condition,\ K} \\ T_{\rm p} & {\rm drilling\ fluid\ temperature\ inside\ the\ drill\ string,\ K}} \\ U & {\rm internal\ energy,\ J/kg} \\ v & {\rm velocity,\ m/s} \\ v_{\infty} & {\rm gas\ slip\ rate,\ m/s} \\ v_{\rm c} & {\rm gas\ characteristic\ velocity,\ m/s} \\ z & {\rm gas\ compressibility\ factor} \\ z_{\rm e} & {\rm gas\ compressibility\ factor\ under\ reservoir\ environment} \\ \beta_{\rm T} & {\rm thermal\ expansion\ coefficient\ of\ the\ pore\ fluid,\ K^{-1}} \\ \gamma & {\rm decreasing\ term} \\ \Delta & {\rm roughness\ of\ the\ pipe\ wall} \\ \theta & {\rm well\ inclination\ angle,\ rad} \\ \lambda & {\rm thermal\ conductivity,\ W/(m\cdot K)} \\ \mu & {\rm viscosity,\ Pa\cdot s} \\ \rho & {\rm density,\ Pa\cdot s} \\ \theta & {\rm density,\ kg/m^3} \\ Subscript \\ g & {\rm gas} \\ 1 & {\rm drilling\ fluid} \\ {\rm s\ hollow\ ball} \\ m & {\rm gas-liquid\text{-}solid\ mixed\ fluid} \\ f & {\rm formation} \\ \end{array}$		<u> </u>
$ \begin{array}{lll} T_{\rm e} & {\rm reservoir\ temperature,\ ^{\circ}C} \\ T_{\rm in} & {\rm temperature\ of\ the\ injected\ drilling\ fluid,\ K} \\ T_{\rm norm} & {\rm wellbore\ temperature\ under\ normal\ condition,\ K} \\ T_{\rm p} & {\rm drilling\ fluid\ temperature\ inside\ the\ drill\ string,\ K} \\ U & {\rm internal\ energy,\ J/kg} \\ v & {\rm velocity,\ m/s} \\ v_{\infty} & {\rm gas\ slip\ rate,\ m/s} \\ v_{\rm c} & {\rm gas\ characteristic\ velocity,\ m/s} \\ z & {\rm gas\ characteristic\ velocity,\ m/s} \\ z & {\rm gas\ compressibility\ factor} \\ z_{\rm e} & {\rm gas\ compressibility\ factor\ under\ reservoir\ environment} \\ \beta_{\rm T} & {\rm thermal\ expansion\ coefficient\ of\ the\ pore\ fluid,\ K^{-1}} \\ \gamma & {\rm decreasing\ term} \\ \Delta & {\rm roughness\ of\ the\ pipe\ wall} \\ \theta & {\rm well\ inclination\ angle,\ rad} \\ \lambda & {\rm thermal\ conductivity,\ W/(m\cdot K)} \\ \mu & {\rm viscosity,\ Pa\cdot s} \\ \rho & {\rm density,\ Pa\cdot s} \\ \theta & {\rm density,\ kg/m^3} \\ Subscript \\ g & {\rm gas} \\ 1 & {\rm drilling\ fluid} \\ {\rm s} & {\rm hollow\ ball} \\ {\rm m} & {\rm gas-liquid-solid\ mixed\ fluid} \\ f & {\rm formation} \\ \end{array}$		·
$\begin{array}{lll} T_{\rm in} & {\rm temperature~of~the~injected~drilling~fluid,~K} \\ T_{\rm norm} & {\rm wellbore~temperature~under~normal~condition,~K} \\ T_{\rm p} & {\rm drilling~fluid~temperature~inside~the~drill~string,~K} \\ U & {\rm internal~energy,~J/kg} \\ v & {\rm velocity,~m/s} \\ v_{\infty} & {\rm gas~slip~rate,~m/s} \\ v_{\rm c} & {\rm gas~characteristic~velocity,~m/s} \\ z & {\rm gas~compressibility~factor} \\ z_{\rm e} & {\rm gas~compressibility~factor~under~reservoir~environment} \\ \beta_{\rm T} & {\rm thermal~expansion~coefficient~of~the~pore~fluid,~K^{-1}} \\ \gamma & {\rm decreasing~term} \\ \Delta & {\rm roughness~of~the~pipe~wall} \\ \theta & {\rm well~inclination~angle,~rad} \\ \lambda & {\rm thermal~conductivity,~W/(m\cdot K)} \\ \mu & {\rm viscosity,~Pa\cdot s} \\ \rho & {\rm density,~kg/m^3} \\ Subscript \\ g & {\rm gas} \\ 1 & {\rm drilling~fluid} \\ s & {\rm hollow~ball} \\ m & {\rm gas-liquid-solid~mixed~fluid} \\ f & {\rm formation} \\ \end{array}$		
$\begin{array}{lll} T_{\rm norm} & \mbox{wellbore temperature under normal condition, K} \\ T_{\rm p} & \mbox{drilling fluid temperature inside the drill string, K} \\ U & \mbox{internal energy, } \mbox{J/kg} \\ v & \mbox{velocity, } m/s \\ v_{\infty} & \mbox{gas slip rate, } m/s \\ v_{\rm c} & \mbox{gas characteristic velocity, } m/s \\ z & \mbox{gas compressibility factor} \\ z_{\rm e} & \mbox{gas compressibility factor under reservoir environment} \\ \beta_{\rm T} & \mbox{thermal expansion coefficient of the pore fluid, K}^{-1} \\ \gamma & \mbox{decreasing term} \\ \Delta & \mbox{roughness of the pipe wall} \\ \theta & \mbox{well inclination angle, rad} \\ \lambda & \mbox{thermal conductivity, W/(m \cdot K)} \\ \mu & \mbox{viscosity, Pa \cdot s} \\ \rho & \mbox{density, kg/m}^3 \\ \mbox{Subscript} \\ g & \mbox{gas} \\ 1 & \mbox{drilling fluid} \\ s & \mbox{hollow ball} \\ m & \mbox{gas-liquid-solid mixed fluid} \\ f & \mbox{formation} \\ \end{array}$		•
$T_{ m p}$ drilling fluid temperature inside the drill string, K U internal energy, $J/k{ m g}$ V velocity, $m/{ m s}$ V_{∞} gas slip rate, $m/{ m s}$ $V_{\rm c}$ gas characteristic velocity, $m/{ m s}$ Z gas compressibility factor $Z_{ m e}$ gas compressibility factor under reservoir environment thermal expansion coefficient of the pore fluid, K^{-1} Y decreasing term $Y_{\rm c}$ $Y_{\rm c}$ decreasing term $Y_{\rm c}$ $Y_{\rm c$		
$\begin{array}{lll} U & \text{internal energy, J/kg} \\ v & \text{velocity, m/s} \\ v_{\infty} & \text{gas slip rate, m/s} \\ v_{\text{c}} & \text{gas characteristic velocity, m/s} \\ z & \text{gas compressibility factor} \\ z_{\text{e}} & \text{gas compressibility factor under reservoir environment} \\ \beta_{\text{T}} & \text{thermal expansion coefficient of the pore fluid, K}^{-1} \\ \gamma & \text{decreasing term} \\ \Delta & \text{roughness of the pipe wall} \\ \theta & \text{well inclination angle, rad} \\ \lambda & \text{thermal conductivity, W/(m \cdot \text{K})} \\ \mu & \text{viscosity, Pa \cdot s} \\ \rho & \text{density, kg/m}^3 \\ \text{Subscript} \\ g & \text{gas} \\ 1 & \text{drilling fluid} \\ \text{s} & \text{hollow ball} \\ \text{m} & \text{gas-liquid-solid mixed fluid} \\ \text{f} & \text{formation} \\ \end{array}$	I norm	
$\begin{array}{cccccccccccccccccccccccccccccccccccc$		
$\begin{array}{lll} v_{\infty} & & \text{gas slip rate, m/s} \\ v_{c} & & \text{gas characteristic velocity, m/s} \\ z & & \text{gas compressibility factor} \\ z_{e} & & \text{gas compressibility factor under reservoir environment} \\ \beta_{T} & & \text{thermal expansion coefficient of the pore fluid, K}^{-1} \\ \gamma & & \text{decreasing term} \\ \Delta & & \text{roughness of the pipe wall} \\ \theta & & \text{well inclination angle, rad} \\ \lambda & & \text{thermal conductivity, W}/(\text{m}\cdot\text{K}) \\ \mu & & \text{viscosity, Pa} \cdot \text{s} \\ \rho & & \text{density, kg/m}^{3} \\ \text{Subscript} \\ g & & \text{gas} \\ 1 & & & \text{drilling fluid} \\ \text{s} & & & \text{hollow ball} \\ \text{m} & & & & \text{gas-liquid-solid mixed fluid} \\ f & & & & & & & & & & & & & & & & & &$		
$\begin{array}{cccccccccccccccccccccccccccccccccccc$		
$ \begin{array}{cccccccccccccccccccccccccccccccccccc$		
$ \begin{array}{cccccccccccccccccccccccccccccccccccc$		
$\begin{array}{lll} \beta_{\rm T} & \text{thermal expansion coefficient of the pore fluid, K}^{-1} \\ \gamma & \text{decreasing term} \\ \Delta & \text{roughness of the pipe wall} \\ \theta & \text{well inclination angle, rad} \\ \lambda & \text{thermal conductivity, W}/(\text{m} \cdot \text{K}) \\ \mu & \text{viscosity, Pa} \cdot \text{s} \\ \rho & \text{density, kg/m}^3 \\ \text{Subscript} \\ \text{g} & \text{gas} \\ 1 & \text{drilling fluid} \\ \text{s} & \text{hollow ball} \\ \text{m} & \text{gas-liquid-solid mixed fluid} \\ \text{f} & \text{formation} \end{array}$		
$\begin{array}{lll} \gamma & & \text{decreasing term} \\ \Delta & & \text{roughness of the pipe wall} \\ \theta & & \text{well inclination angle, rad} \\ \lambda & & \text{thermal conductivity, W/(m·K)} \\ \mu & & \text{viscosity, Pa·s} \\ \rho & & \text{density, kg/m}^3 \\ \text{Subscript} \\ g & & \text{gas} \\ 1 & & \text{drilling fluid} \\ s & & \text{hollow ball} \\ m & & \text{gas-liquid-solid mixed fluid} \\ f & & \text{formation} \end{array}$		
$\begin{array}{lll} \Delta & \text{roughness of the pipe wall} \\ \theta & \text{well inclination angle, rad} \\ \lambda & \text{thermal conductivity, W/(m·K)} \\ \mu & \text{viscosity, Pa·s} \\ \rho & \text{density, kg/m}^3 \\ \text{Subscript} \\ g & \text{gas} \\ 1 & \text{drilling fluid} \\ s & \text{hollow ball} \\ m & \text{gas-liquid-solid mixed fluid} \\ f & \text{formation} \end{array}$		
$\begin{array}{lll} \theta & \text{well inclination angle, rad} \\ \lambda & \text{thermal conductivity, W/(m·K)} \\ \mu & \text{viscosity, Pa-s} \\ \rho & \text{density, kg/m}^3 \\ \text{Subscript} \\ \text{g} & \text{gas} \\ \text{I} & \text{drilling fluid} \\ \text{s} & \text{hollow ball} \\ \text{m} & \text{gas-liquid-solid mixed fluid} \\ \text{f} & \text{formation} \end{array}$	•	•
$\begin{array}{lll} \lambda & & \text{thermal conductivity, W/(m\cdot K)} \\ \mu & & \text{viscosity, Pa\cdot s} \\ \rho & & \text{density, kg/m}^3 \\ \text{Subscript} & & & & & \\ g & & & & & \\ 1 & & & & & \\ 1 & & & & & \\ s & & & & & \\ hollow \ ball & & & \\ m & & & & & \\ gas-liquid-solid \ mixed \ fluid \\ f & & & & \\ \end{array}$		
$\begin{array}{lll} \mu & \text{viscosity, Pa·s} \\ \rho & \text{density, kg/m}^3 \\ \text{Subscript} \\ \text{g} & \text{gas} \\ \text{I} & \text{drilling fluid} \\ \text{s} & \text{hollow ball} \\ \text{m} & \text{gas-liquid-solid mixed fluid} \\ \text{f} & \text{formation} \end{array}$	-	
ρ density, kg/m³ Subscript g gas I drilling fluid s hollow ball m gas-liquid-solid mixed fluid f formation		
Subscript g gas l drilling fluid s hollow ball m gas-liquid-solid mixed fluid f formation	'	
g gas I drilling fluid s hollow ball m gas-liquid-solid mixed fluid f formation		density, kg/m²
I drilling fluid s hollow ball m gas-liquid-solid mixed fluid f formation	-	
s hollow ball m gas-liquid-solid mixed fluid f formation		
m gas-liquid-solid mixed fluid f formation	=	
f formation	S	
		• .
pl pore fluid		
	pl	pore fluid

References

- Al Saedi, A.Q., Flori, R.E., Kabir, C.S., 2018. New analytical solutions of wellbore fluid temperature profiles during drilling, circulating, and cementing operations. J. Pet. Sci. Eng. 170, 206–217. https://doi.org/10.1016/j.petrol.2018.06.027.
- Avelar, C.S., Ribeiro, P.R., Sepehrnoori, K., 2009. Deepwater gas kick simulation. J. Pet. Sci. Eng. 67 (1–2), 13–22. https://doi.org/10.1016/j.petrol.2009.03.001.
- Bhagwat, S.M., Ghajar, A.J., 2014. A flow pattern independent drift flux model based void fraction correlation for a wide range of gas—liquid two phase flow. Int. J. Multiphas. Flow 59, 186—205. https://doi.org/10.1016/j.ijmultiphaseflow.2013.11.001.
- Chen, N.H., 1979. An explicit equation for friction factor in pipe. Ind. Eng. Chem. Fundam. 18 (3), 296–297. https://doi.org/10.1021/i160071a019.
- Chen, X.Y., Yang, J., Gao, D.L., Huang, Y., Li, Y.J., Luo, M., Li, W.T., 2018. Well control for offshore high-pressure/high-temperature highly deviated gas wells drilling: how to determine the kick tolerance?. In: IADC/SPE Asia Pacific Drilling Technology Conference and Exhibition. SPE-190969-MS. https://doi.org/10.2118/ 190969-MS.
- Choe, J., Schubert, J.J., Juvkam-Wold, H.C., 2007. Analyses and procedures for kick detection in subsea mudlift drilling. SPE Drill. Complet. 22 (4), 296–303. https://doi.org/10.2118/87114-PA.
- Choi, J., Pereyra, E., Sarica, C., Lee, H., Jang, I.S., Kang, J., 2013. Development of a fast transient simulator for gas—liquid two-phase flow in pipes. J. Pet. Sci. Eng. 102, 27—35. https://doi.org/10.1016/j.petrol.2013.01.006.
- Davoudi, M., Smith, J.R., Patel, B.M., Chirinos, J.E., 2011. Evaluation of alternative initial responses to kicks taken during managed-pressure drilling. SPE Drill. Complet. 26 (2), 169–181. https://doi.org/10.2118/128424-PA.
- Dixit, A., ElSheikh, A.H., 2022. Stochastic optimal well control in subsurface reservoirs using reinforcement learning. Eng. Appl. Artif. Intell. 114, 105106. https://doi.org/10.1016/j.engappai.2022.105106.
- Dou, L.B., Li, G.S., Shen, Z.H., Song, X.Z., Chi, H.P., Du, T., 2012. Study on the well control safety during formation high-sulfur gas invasion. In: IADC/SPE Asia Pacific Drilling Technology Conference and Exhibition. SPE-156322-MS. https:// doi.org/10.2118/156322-MS.
- Ekrann, S., Rommetveit, R., 1985. A simulator for gas kicks in oil-based drilling muds. In: SPE Annual Technical Conference and Exhibition. SPE-14182-MS. https://doi.org/10.2118/14182-MS.
- Farahani, H.S., Yu, M., Miska, S., Takach, N., Chen, G., 2006. Modeling transient thermo-poroelastic effects on 3D wellbore stability. In: SPE Annual Technical Conference and Exhibition. SPE-103159-MS. https://doi.org/10.2118/103159-MS.
- Gao, D.L., Zhu, W.X., Li, J., Zhang, J.W., Meng, Q.F., 2016. Scientific problems and technical bottlenecks in deepwater oil & gas engineering—academic review of the 147th Shuangqing Forum. China Basic Sci 18 (3), 1–6. https://doi.org/ 10.3969/j.issn.1009-2412.2016.03.001 (in Chinese).
- Gao, Y.H., Sun, X.H., Zhao, T.H., Wang, Z.Y., Zhao, X.X., Sun, B.J., 2018. Study on the migration of gas kicks in undulating sections of horizontal wells. Int. J. Heat Mass Tran. 127, 1161–1167. https://doi.org/10.1016/j.ijheatmasstransfer.2018.07.156.
- Gomes, D., Frøyen, J., Fjelde, K.K., Bjørkevoll, K., 2018. A numerical comparison and uncertainty analysis of two transient models for kick management in a backpressure MPD system. In: SPE Norway Subsurface Conference. SPE-191345-MS. https://doi.org/10.2118/191345-MS.
- He, M., Xu, M.B., Li, J., Liu, G.H., 2017. A new two-phase model to simulate sour gas kicks in MPD operations with water based mud. J. Pet. Sci. Eng. 159, 331–343. https://doi.org/10.1016/j.petrol.2017.09.015.
- Hibiki, T., Ju, P., Rassame, S., Miwa, S., Shen, X.Z., Ozaki, T., 2022. Channel size effect on drift-flux parameters for adiabatic and boiling two-phase flows. Int. J. Heat Mass Tran. 185, 122410. https://doi.org/10.1016/j.jiheatmasstransfer.2021.122410.
- Jiang, H., Liu, G.H., Li, J., Zhang, T., Wang, C., Ren, K., 2019. Numerical simulation of a new early gas kick detection method using UKF estimation and GLRT. J. Pet. Sci. Eng. 173, 415–425. https://doi.org/10.1016/j.petrol.2018.09.065.
- Johnson, A.B., Cooper, S., 1993. Gas migration velocities during gas kicks in deviated wells. In: SPE Annual Technical Conference and Exhibition. SPE-26331-MS. https://doi.org/10.2118/26331-MS.
- Kaasa, G.O., Stamnes, Ø.N., Imsland, L., Aamo, O.M., 2012. Simplified hydraulics model used for intelligent estimation of downhole pressure for a managedpressure-drilling control system. SPE Drill. Complet. 27 (1), 127–138. https:// doi.org/10.2118/143097-PA.
- Karimi Vajargah, A., Miska, S.Z., Yu, M., Ozbayoglu, M.E., Majidi, R., 2013. Feasibility study of applying intelligent drill pipe in early detection of gas influx during conventional drilling. In: SPE/IADC Drilling Conference and Exhibition. SPE-163445-MS. https://doi.org/10.2118/163445-MS.
- Kinik, K., Gumus, F., Osayande, N., 2015. Automated dynamic well control with managed-pressure drilling: a case study and simulation analysis. SPE Drill. Complet. 30 (2), 110–118. https://doi.org/10.2118/168948-PA.
- Li, X., Zhang, J., Tang, X., Li, C.N., Li, B., Wang, Y., Zhao, Z.P., 2022. Propagation characteristics and application effects of measurement-while-drilling pressure wave for early gas-kick detection. J. Loss Prev. Process. Ind. 76, 104741. https://doi.org/10.1016/j.jlp.2022.104741.
- Livescu, S., Durlofsky, L.J., Aziz, K., Ginestra, J.C., 2010. A fully-coupled thermal multiphase wellbore flow model for use in reservoir simulation. J. Pet. Sci. Eng.

- 71 (3-4), 138-146. https://doi.org/10.1016/j.petrol.2009.11.022.
- Lopes, C.A., 1997. Feasibility Study on the Reduction of Hydrostatic Pressure in a Deep-Water Riser Using a Gas-Lift Method. PhD Thesis. Louisiana State University and Agricultural & Mechanical College.
- Lorentzen, R.J., Fjelde, K.K., Frøyen, J., Lage, A.C., Nævdal, G., Vefring, E.H., 2001.

 Underbalanced and low-head drilling operations: real time interpretation of measured data and operational support. In: SPE Annual Technical Conference and Exhibition. SPE-71384-MS. https://doi.org/10.2118/71384-MS.
- Nas, S., 2011. Kick detection and well control in a closed wellbore. In: SPE/IADC Managed Pressure Drilling and Underbalanced Operations Conference and Exhibition. SPE-143099-MS. https://doi.org/10.2118/143099-MS.
- Nas, S., Gedge, B., Palao, F., Viet Bot, N., 2010. Advantages of managed pressure drilling and the recent deployment of the technology in Vietnam. In: IADC/SPE Asia Pacific Drilling Technology Conference and Exhibition. SPE-136513-MS. https://doi.org/10.2118/136513-MS.
- Nayeem, A.A., Venkatesan, R., Khan, F., 2016. Monitoring of down-hole parameters for early kick detection. J. Loss Prev. Process. Ind. 40, 43–54. https://doi.org/ 10.1016/j.jlp.2015.11.025.
- Nunes, J.O.L., Bannwart, A.C., Ribeiro, P.R., 2002. Mathematical modeling of gas kicks in deep water scenario. In: IADC/SPE Asia Pacific Drilling Technology Conference and Exhibition. SPE-77253-MS, https://doi.org/10.2118/77253-MS.
- Santos, H., Leuchtenberg, C., Shayegi, S., 2003. Micro-flux control: the next generation in drilling process. In: SPE Latin America and Caribbean Petroleum Engineering Conference. SPE-81183-MS. https://doi.org/10.2118/81183-MS.
- Schubert, J., Choe, J., Dreher, D., Juvkam-Wold, H., 2006. Analysis of gas kicks in multilateral wells utilizing computer simulation. In: SPE/IADC Drilling Conference and Exhibition. SPE-99028-MS. https://doi.org/10.2118/99028-MS.
- Shi, H., Holmes, J.A., Durlofsky, L.J., Aziz, K., Diaz, L.R., Alkaya, B., Oddie, G., 2005. Drift-flux modeling of two-phase flow in wellbores. SPE J. 10 (1), 24–33. https://doi.org/10.2118/84228-PA.
- Smith, J.R., Patel, B.M., 2012. A proposed method for planning the best initial response to kicks taken during managed-pressure-drilling operations. SPE Drill. Complet. 27 (2), 194–203. https://doi.org/10.2118/143101-PA.
 Sun, B.J., Fu, W.Q., Wang, N., Wang, Z.Y., Gao, Y.H., 2019. Multiphase flow modeling
- Sun, B.J., Fu, W.Q., Wang, N., Wang, Z.Y., Gao, Y.H., 2019. Multiphase flow modeling of gas intrusion in oil-based drilling mud. J. Pet. Sci. Eng. 174, 1142–1151. https:// doi.org/10.1016/j.petrol.2018.12.018.Sun, B.J., Sun, X.H., Wang, Z.Y., Chen, Y.H., 2017. Effects of phase transition on gas
- Sun, B.J., Sun, X.H., Wang, Z.Y., Chen, Y.H., 2017. Effects of phase transition on gas kick migration in deepwater horizontal drilling. J. Nat. Gas Sci. Eng. 46, 710–729. https://doi.org/10.1016/j.jngse.2017.09.001.
- Sun, X.H., Sun, B.J., Gao, Y.H., Wang, Z.Y., 2018. A model of multiphase flow dynamics considering the hydrated bubble behaviors and its application to deepwater kick simulation. J. Energy Resour. Technol. 140 (8), 082004. https://doi.org/ 10.1115/1.4040190.
- Sunthankar, A.A., Kuru, E., Miska, S., Kamp, A., 2001. New developments in aerated mud hydraulics for drilling in inclined wells. In: SPE Oklahoma City Oil and Gas Symposium/Production and Operations Symposium. SPE-67189-MS. https:// doi.org/10.2118/67189-MS.
- Tang, H.W., Rashid Hasan, A., Killough, J., 2018. Development and application of a fully implicitly coupled wellbore/reservoir simulator to characterize the transient liquid loading in horizontal gas wells. SPE J. 23 (5), 1615–1629. https:// doi.org/10.2118/187354-PA.
- Wang, N., Wang, J.B., Sun, B.J., Wang, Z.Y., Li, H., 2016. Study of transient responses in the APWD measurements during gas influx. J. Nat. Gas Sci. Eng. 35, 522–531. https://doi.org/10.1016/j.jngse.2016.08.057.
- Xu, Z.M., Song, X.Z., Li, G.S., Wu, K., Pang, Z.Y., Zhu, Z.P., 2018. Development of a transient non-isothermal two-phase flow model for gas kick simulation in HTHP deep well drilling. Appl. Therm. Eng. 141, 1055–1069. https://doi.org/ 10.1016/j.applthermaleng.2018.06.058.
- Yang, H.W., Li, J., Jiang, J.W., Zhang, H., Guo, B.Y., Zhang, G., Chen, W., 2022a. A dynamic managed pressure well-control method for rapid treatment of gas kick in deepwater managed pressure drilling. Petrol. Sci. 19 (5), 2297–2313. https://doi.org/10.1016/j.petsci.2022.06.011.
- Yang, H.W., Li, J., Liu, G.H., Xing, X., Jiang, H.L., Wang, C., 2020. The effect of interfacial mass transfer of slip-rising gas bubbles on two-phase flow in the vertical wellbore/pipeline. Int. J. Heat Mass Tran. 150, 119326. https://doi.org/10.1016/j.ijheatmasstransfer.2020.119326.
- Yang, H.W., Li, J., Zhang, H., Liu, G.H., Zhang, G., Guo, B., 2022b. Physical experiment on the feasibility of variable-gradient drilling method based on downhole separator. Energy Rep. 8, 1591–1601. https://doi.org/10.1016/j.egyr.2021.12.074.
- Yang, X., Meng, Y.F., Shi, X.C., Li, G., 2017. Influence of porosity and permeability heterogeneity on liquid invasion in tight gas reservoirs. J. Nat. Gas Sci. Eng. 37, 169–177. https://doi.org/10.1016/j.jngse.2016.11.046.
- Yin, B.T., Liu, G., Li, X.F., 2017. Multiphase transient flow model in wellbore annuli during gas kick in deepwater drilling based on oil-based mud. Appl. Math. Model. 51, 159–198. https://doi.org/10.1016/j.apm.2017.06.029.
- Yin, Q.S., Yang, J., Tyagi, M., Zhou, X., Wang, N., Tong, G., Xie, R.J., Liu, H.X., Cao, B.H., 2022. Downhole quantitative evaluation of gas kick during deepwater drilling with deep learning using pilot-scale rig data. J. Pet. Sci. Eng. 208, 109136. https://doi.org/10.1016/j.petrol.2021.109136.
- Zachopoulos, F., Kokkinos, N., 2023. Mathematical modeling of oil and gas kick during drilling operations. AIP Conf. Proc. 2872 (1), 020004. https://doi.org/

10.1063/5.0165932.
Zhang, G.Y., Ma, F., Liang, Y.B., Zhao, Z., Qin, Y.Q., Liu, X.B., Zhang, K.B., Ke, W.L., 2015.
Domain and theory-technology progress of global deep oil & gas exploration.
Acta Petrol. Sin. 36 (9), 1156–1166. https://doi.org/10.7623/syxb201509015 (in

Zhang, X.L., Ding, T.B., Zhou, B., Yin, B.T., 2024. Mechanism of displacement gas kick

in horizontal well drilling into deep fractured gas reservoir. Front. Energy Res. 12, 1412038. https://doi.org/10.3389/fenrg.2024.1412038.

Zuber, N., Findlay, J.A., 1965. Average volumetric concentration in two-phase flow systems. ASME J. Heat Mass Transf 87 (4), 453—468. https://doi.org/10.1115/ 1.3689137.